iScience

CellPress
OPEN ACCESS

Article

Nanosphere pharmacodynamics improves safety of immunostimulatory cytokine therapy

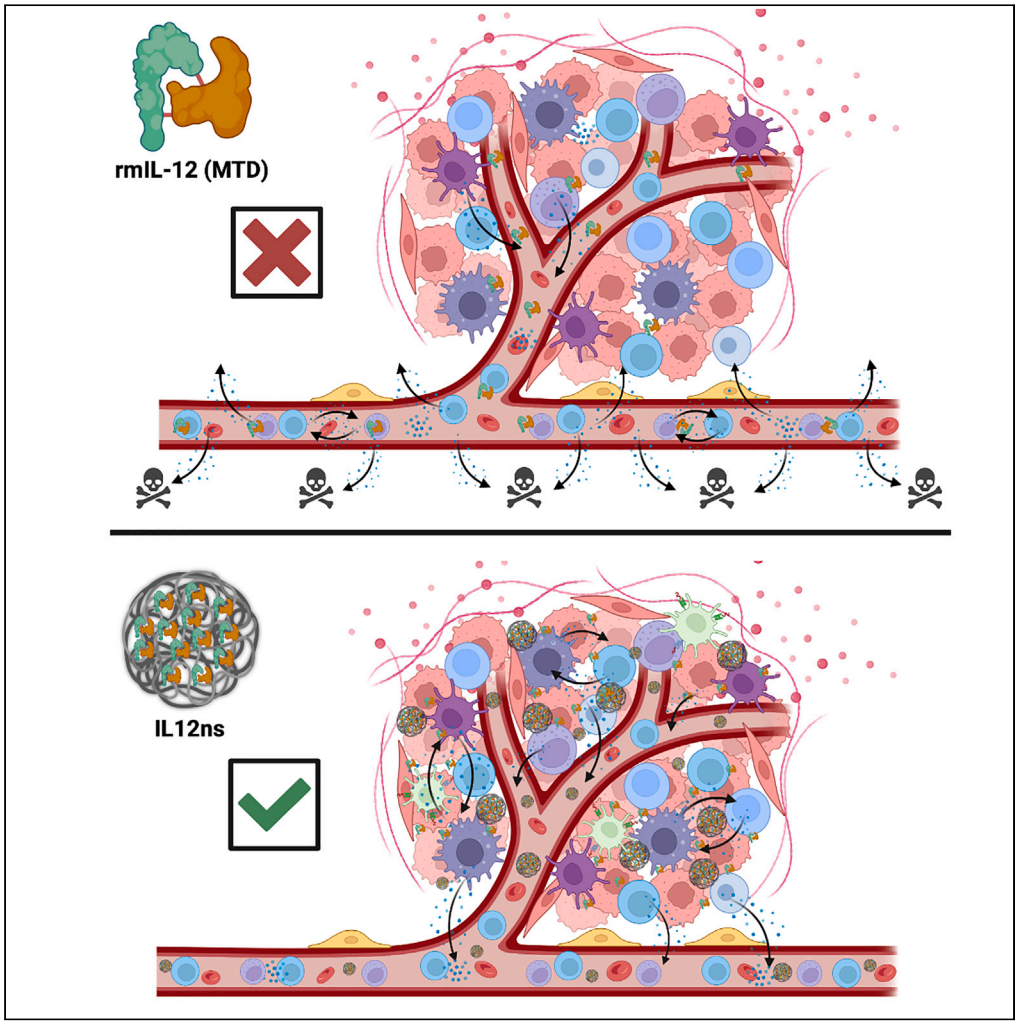

Ryan A. Lacinski, Sebastian A. Dziadowicz, Amanda Stewart, ..., Ana de Oliveira, Stell P. Santiago, Brock A. Lindsey

blinds10@jh.edu

Highlights

Immunotoxicology assessment of IL12ns with a rigorous immune diagnostic platform

IL12ns prevents peripheral blood stimulation but drives local tissue inflammation

Necessity of vector-based delivery for safe immunostimulatory therapy supported

Lacinski et al., iScience 27, 108836
February 16, 2024
https://doi.org/10.1016/j.isci.2024.108836

iScience

CellPress
OPEN ACCESS

Article

Nanosphere pharmacodynamics improves safety of immunostimulatory cytokine therapy

Ryan A. Lacinski,[1] Sebastian A. Dziadowicz,[2,3] Amanda Stewart,[1] Edwin Chaharbakhshi,[1] Halima Akhter,[2,3] John J. Pisquiy,[1] Jack H. Victory,[1] Joshua B. Hardham,[1] Claude Chew,[4] Alyson Prorock,[5] Yongde Bao,[5] Katia Sol-Church,[5] Gerald R. Hobbs,[1] Edwin Klein,[6] Michael A. Nalesnik,[7] Gangqing Hu,[2,3] Ana de Oliveira,[8] Stell P. Santiago,[9] and Brock A. Lindsey[10,11,*]

SUMMARY

Systemic administration of interleukin (IL)-12 induces potent anti-tumor immune responses in preclinical cancer models through the systemic activation of effector immune cells and release of proinflammatory cytokines. IL-12-loaded PLGA nanospheres (IL12ns) are hypothesized to improve therapeutic efficacy and thwart unwanted side effects observed in previous human clinical trials. Through the investigation of peripheral blood and local tissue immune responses in healthy BALB/c mice, the immune-protective pharmacodynamics of IL12ns were suggested. Nanospheres increased pro-inflammatory plasma cytokines/chemokines (IFN-γ, IL-6, TNF-α, and CXCL10) without inducing maladaptive transcriptomic signatures in circulating peripheral immune cells. Gene expression profiling revealed activation of pro-inflammatory signaling pathways in systemic tissues, the likely source of these effector cytokines. These data support that nanosphere pharmacodynamics, including shielding IL-12 from circulating immune cells, depositing peripherally in systemic immune tissues, and then slowly eluting bioactive cytokine, thereafter, are essential to safe immunostimulatory therapy.

INTRODUCTION

While the immune surveillance and cancer immunoediting theories are well understood phenomena,[1] their impact on the development of immunotherapies has been limited. The cornerstone of these theories is that an immunosurveillance-like state must be maximized to overcome the constitutive immunosuppression seen in cancer patients. In essence, immunotherapies would then promote the elimination of tumor cells through enhanced effector immune responses driven by overcoming this unbalanced cancer-immune cell equilibrium.[2–4] Targeted immunotherapeutic treatments have been proposed to avoid immunologic toxicity (immunotoxicity) while maintaining therapeutic efficacy. Unfortunately, pleiomorphic tumors are often capable of downregulating the presentation of the associated target antigens. These tumor-immune escape mechanisms thereby limit effective immune responses and overall efficacy.[5,6] Even if these immunosuppressive interactions are blocked, the immune system often requires an additional stimulus to create the pro-inflammatory and supra-normal immune response required for tumor cell cytotoxicity. Systemic administration of interleukin (IL)-12 has been proposed to induce these desired anti-tumor immune responses.[7–9]

IL-12 is an immunostimulatory cytokine with a well-documented history of anti-tumor activity in preclinical cancerous models.[7–15] This pro-inflammatory cytokine is a key regulator of cell-mediated immune responses and is produced endogenously by dendritic cells, monocytes, and M1-like macrophages.[16] Binding of IL-12 to its type 1 cytokine surface receptor[17] influences cellular differentiation of T helper cells into a Th1 phenotype. These cells can then coordinate adaptive antitumor immunity through further activation of cytotoxic T cells, Natural Killer (NK) cells, and pro-inflammatory M1-like macrophages, resulting in the downstream release of interferons (IFNs) such as IFN-γ.[18] IL-12 mediated increases in both CXCL9-10 are associated with its strong anti-angiogenic properties and proposed ability to reduce cancer metastasis.[19] Importantly, preclinical studies have consistently suggested that IL-12's antitumor effects are most evident when given systemically as

[1]Department of Orthopaedics, West Virginia University School of Medicine, Morgantown, WV 26505, USA
[2]Department of Microbiology, Immunology, and Cell Biology, West Virginia University School of Medicine, Morgantown, WV 26505, USA
[3]Bioinformatics Core, West Virginia University School of Medicine, Morgantown, WV 26505, USA
[4]Advanced Technology Cores, Baylor College of Medicine, Houston, TX 77030, USA
[5]Genome Analysis & Technology Core, University of Virginia School of Medicine, Charlottesville, VA 22904, USA
[6]Division of Laboratory Animal Resources, University of Pittsburgh School of Medicine, Pittsburgh, PA 15260, USA
[7]Department of Pathology, University of Pittsburgh Medical Center, Pittsburgh, PA 15260, USA
[8]Department of Pathology, University of Virginia School of Medicine, Charlottesville, VA 22904, USA
[9]Department of Pathology, West Virginia University School of Medicine, Morgantown, WV 26505, USA
[10]Department of Orthopaedic Surgery, Johns Hopkins University School of Medicine, Baltimore, MD 21287, USA
[11]Lead contact
*Correspondence: blinds10@jh.edu
https://doi.org/10.1016/j.isci.2024.108836

opposed to locally via intratumoral delivery. This finding is particularly due to the observed increases in systemic immune cell activation, production of proinflammatory, effector cytokines, and indirect inhibition of pro-tumoral angiogenesis.[20]

While these initial preclinical data were promising, clinical trials using intravenous (i.v.) recombinant human IL-12 (rhIL-12) concluded that bolus IL-12 injection exhibited limited therapeutic efficacy.[21,22] This limited efficacy was associated with signs of clinical toxicity including lymphopenia and elevated liver enzymes. Signs of immunotoxicity, evidenced by the reduction in serum IFN-γ levels with continued treatment, were also evident.[21,23–27] Importantly, dosing strategies for cytokine-based immunotherapies developed in the late 1990s were influenced by approaches deployed for cytotoxic chemotherapy at this time. While still vitally important to monitor for signs of clinical toxicity during treatment, a maximal tolerable dosing (MTD) strategy likely does not translate to treatment with immunotherapies.[28]

While supranormal doses of IL-12 greater than natural, endogenous levels are arguably necessary for anti-tumor efficacy, strategies to both reduce the required loading dose and monitor the immune-related changes associated with immunostimulatory therapies are critical for their clinical efficacy. To address these barriers, we successfully developed IL-12-loaded PLGA nanospheres (IL12ns) that release their contents systemically in a slow and controlled manner.[29–31] A previously published *in vivo* assessment of single-dose IL12ns treatment revealed that nanospheres may not produce the exhaustive cytokinome associated with previous clinical trial failures.[31] This work was then followed by extensive *in vitro* efforts to improve nanosphere encapsulation efficiency and fabrication yields via a modified sonication-based synthesis approach. The newly synthesized nanospheres were then validated to elute bioactive IL-12 through an *ex vivo* immunostimulatory assay. Here, results suggested no difference in ED_{50} of eluted IL-12 (from nanospheres) versus stock, unencapsulated IL-12 controls, supporting no change in protein bioactivity with the improved fabrication process. Subsequently, a trial investigating weekly IL12ns treatment in our murine model of metastatic osteosarcoma depicted the greatest reduction in disease progression (metastatic and/or recurrent disease) with the lowest dose tested, supporting *in vivo* therapeutic efficacy.[30] These data ultimately suggest that our platform successfully delivers an effective dose of proinflammatory IL-12 to shift the immune equilibrium toward an effector surveillance state, preventing metastatic and recurrent disease progression, as previously suggested.[20]

Ultimately, undesirable toxicity and suboptimal clinical efficacy in previous clinical trials were likely related to inappropriate MTD strategies, route of delivery, and lack of real-time immune monitoring. To achieve effective outcomes with immunostimulatory therapy, there must be a paradigm shift from "tolerable" dosing strategies toward "optimal biologic dosing". This next-generation dosing strategy will require development of adequate immune diagnostic platforms (IDPs). These IDPs must be capable of monitoring therapeutic response through repeated blood sampling and biomarker identification over the course of therapy. Biomarkers would then become the basis of patient-specific dose modulation.[28]

The purpose of this study was to assess the toxicity of the IL12ns vector system in healthy BALB/c mice through repeated blood sampling and organ histological analysis. Both systemic and tissue-resident immune responses to IL12ns therapy, delivered at three doses (10, 0.1, and 0.001 mg), were compared to a daily MTD strategy (10,000 ng/kg/day – positive control) and saline (negative) control. Systemic immunophenotyping with the IDP occurred at designated serial blood sampling timepoints (T) including baseline (T1), 12-h (T2), day 4 (T3), day 8 (T4), day 11 (T5), day 15 (T6), and day 18 (T7). This analysis was followed by both traditional histopathological analysis and targeted gene-expression profiling of euthanasia-harvested tissues (Figure 1). We hypothesized that bolus MTD strategy would recapitulate the immunological findings from previous clinical trials.[23] As opposed to the aberrant peripheral immune overstimulation seen in the MTD cohort, IL12ns was hypothesized to limit peripheral blood pro-inflammatory signaling by shielding IL-12 from peripheral immune cells. Through near immediate tissue deposition of the vector system, IL12ns would then drive local inflammatory responses within tissues. These pro-inflammatory responses would be measured as increases in tissue-related cytokines and chemokines alongside minimal peripheral immune cell activation. The combination of proteomic, transcriptomic, and histopathological assessments would support the necessity of the IL12ns vector system for safe immunostimulatory therapy while further characterizing nanosphere pharmacodynamics.

RESULTS

IL12ns synthesis and characterization

Scanning electron microscopy (SEM) confirmed successful synthesis of IL12ns by the double-emulsion solvent evaporation (DESE) method with modification[30] (Figure S1A). IL12ns elution studies confirmed the release of recombinant murine IL-12 over a 14-day period with minimal elution profile variability, as evidenced by an average standard error of the mean per day (expressed as %) of 8.10% (Figure S1B). IL12ns batches also exhibited consistent and reproducible concentrations (38.08 ± 2.97 mg/mL), yields (152.30 ± 11.86 mg/mL), and encapsulation efficiencies (EE, 35.47 ± 4.79%) (n = 6) (Figure S1C). Dynamic light scattering (DLS) analysis reported a mean diameter of 632.53 ± 65.16 nm and polydispersity index (PDI) of 0.641 ± 0.038 (n = 4) (Figure S1D). Based upon *in vitro* elution studies, the 10, 0.1, and 0.001 mg IL12ns doses delivered approximately 1600, 16, and 0.16 ng/kg of recombinant murine IL-12 per day, respectively.

Spectral flow cytometric analysis of peripheral blood mononuclear cells (PBMCs)

Peripheral blood sampling occurred at designated timepoints (T) including baseline (T1), 12-h (T2), day 4 (T3), day 8 (T4), day 11 (T5), day 15 (T6), and day 18 (T7). Flow cytometric analysis at each timepoint (T), expressed as a percent (%) of all live cells, revealed remarkable immunological differences between experimental groups for both the neutrophil (Figures 1C–1I) and polymorphonuclear (PMN)-myeloid derived suppressor cell (MDSC) populations (Figures 1J–1P). The immunophenotypic markers or genes of interest, and their associated descriptors, identified throughout this manuscript can be found in Table 1. In males, there were significant increases ($p < 0.0001$) in the % neutrophils for

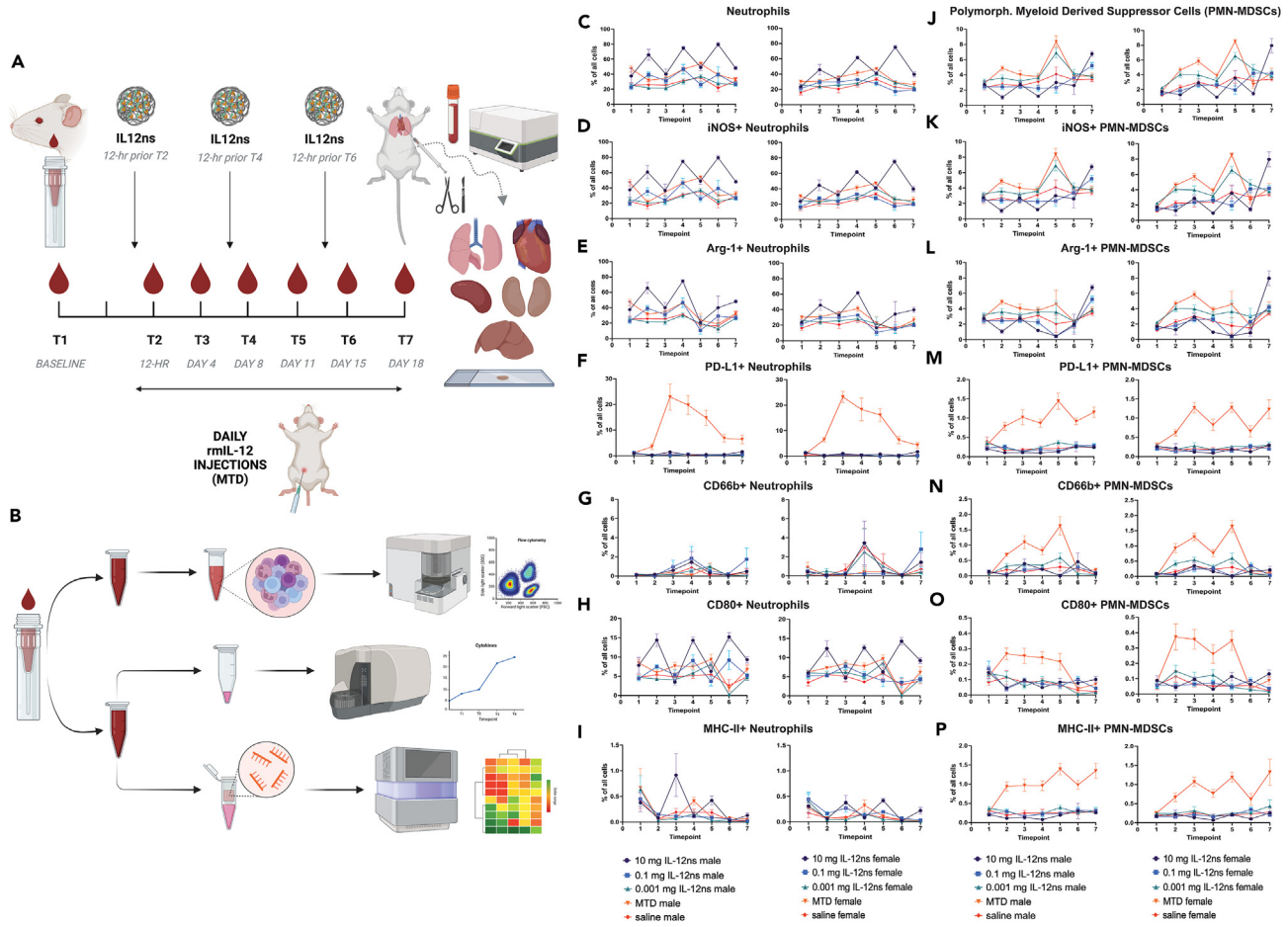

Figure 1. Overview of experimental design

Flow cytometric analysis revealed modulation of myeloid-lineage immune cells with IL-12 treatment.

(A) The resulting systemic immune response from various IL-12 treatment strategies in healthy 7–8-week male/female BALB/c mice was analyzed via seven serial blood sampling timepoints. Timepoints included baseline (T1), 12-h (T2), day 4 (T3), day 8 (T4), day 11 (T5), day 15 (T6), and day 18 (T7), at which time mice were humanely euthanized for full necropsy following cardiac puncture. Experimental mice received either weekly (IL12ns) or daily (MTD) injections at indicated timepoints. At day 18 (T7, euthanasia), peripheral blood was collected via cardiac puncture. This was followed by necropsy to harvest heart, liver, spleen, lungs, and kidneys for histopathological analysis. NanoString nCounter analysis with a custom pro-inflammatory panel was also performed on RNA isolated from the formalin-fixed, paraffin embedded liver, spleen, and lung specimens.

(B) At each sampling timepoint, peripheral blood was collected via cheek bleed (~80 μL) for analysis via an immune diagnostic platform (IDP) consisting of PBMC spectral flow cytometric analysis, plasma cytokine/chemokine analysis, and bulk PBMC RNA-sequencing [Figure by BioRender.com].

(C–P) PBMCs isolated into single cell suspension at serial blood sampling timepoints [baseline (T1), 12-h (T2), day 4 (T3, n = 7 for saline male), day 8 (T4, n = 7 for saline male), day 11 (T5, n = 7 for saline male and 10 mg female), day 15 (T6, n = 7 for saline male and 10 mg female), and day 18 (T7, n = 7 for saline male and 10 mg female)] were analyzed by spectral flow cytometry using the appended gating strategy (Figure S7). Neutrophils (C) were analyzed for expression of iNOS (D), Arg-1 (E), PD-L1 (F), CD66b (G), CD80 (H), and MHC-II (I). Polymorphonuclear myeloid derived suppressor cells (PMN-MDSC) (J) were also analyzed for expression of iNOS (K), Arg-1 (L), PD-L1 (M), CD66b (N), CD80 (O), and MHC-II (P) (male mice – left, female mice – right). Each data point represents the average percent (%) of all (live) cells for each cellular population. Unless indicated above, an n = 8 mice per group per sex were included in the analysis. Where visible, error bars represent standard error of the mean (SE). For visual clarity, findings from statistical analyses can be found in File S1. The x axis represents the timepoint of blood collection while the y axis indicates the % of all (live) cells.

the 10 mg IL12ns group versus all other experimental groups at T4 and T6, with similar trends also persisting at T2. This elevation in neutrophils for the 10 mg IL12ns group increased over time, with the largest % neutrophils evident at T6 (57.7% higher than saline control, 40.5% higher than MTD). This finding was also evident within female mice, particularly at IL12ns-dosing timepoints T4 and T6. Trending increases in % neutrophils for the MTD group compared to saline control were also evident at timepoints T2 and T3 (Figure 1C). Importantly, the increases in % neutrophils are only associated with IL12ns dosing timepoints (T2, T4, and T6) and appear transient in nature, as levels quickly return to near baseline thereafter (T3, T5, and T7). Resultingly, further immunophenotypic characterization of neutrophils from both dosing strategies (MTD, IL12ns) is required to infer their overall immunologic implications.

Table 1. List of immunophenotypic markers or gene IDs, alternative names, and their descriptions

Marker/Gene ID	Description
Abcb11	ATP-binding cassette, sub-family B (MDR/TAP), member 11
Abcb4	ATP-binding cassette, sub-family B (MDR/TAP), member 4
Abcc2	ATP-binding cassette, sub-family C (CFTR/MRP), member 2
Abcc3	ATP-binding cassette, sub-family C (CFTR/MRP), member 3
Alas1	5′-aminolevulinate synthase 1
Anxa2	Annexin A2
Apex1	APEX nuclease (multifunctional DNA repair enzyme) 1
Arg-1 (*Arg1*)	Arginase 1
B2M	Beta-2-microglobulin
Btg2	BTG family, member 2
Casp3	Caspase 3, apoptosis-related cysteine peptidase
CCL2 (MCP-1)	C-C motif chemokine ligand 2 (Monocyte Chemoattractant Protein-1)
CCL3 (MIP-1α)	C-C motif chemokine ligand 3 (Macrophage Inflammatory Protein-1 Alpha)
CCL4 (MIP-1β)	C-C motif chemokine ligand 4 (Macrophage Inflammatory Protein-1 Beta)
CCL5 (RANTES)	C-C Motif Chemokine Ligand 5
Ccng1	Cyclin G1
CCR2 (CD192)	C-C Motif Chemokine Receptor 2
CCR5 (CD195)	Chemokine (C-C Motif) Receptor 5
CD119 (IFNGR1)	Interferon gamma receptor 1
CD11b (*Itgam*)	Integrin subunit alpha M
CD11c (*Itgax*)	Integrin subunit alpha X
CD127 (IL-7Rα)	Interleukin 7 receptor alpha
CD132 (IL2RG)	Interleukin-2 receptor subunit gamma
CD152 (CTLA-4)	Cytotoxic T-lymphocyte-associated protein 4
CD159a (NKG2A)	NK group 2, member A
CD183 (CXCR3)	C-X-C motif chemokine receptor 3
CD19	B-Lymphocyte Surface Antigen B4
CD223 (LAG3)	Lymphocyte-activation gene 3
CD226 (DNAM-1)	DNAX Accessory Molecule-1
CD25 (IL2Rα)	Interleukin-2 receptor alpha chain
CD274 (PD-L1)	Programmed death-ligand 1
CD279 (PD-1)	Programmed cell death protein 1
CD335 (NKp46 or *Ncr1*)	Natural cytotoxicity triggering receptor 1
Cd36	CD36 molecule (thrombospondin receptor)
CD4	Cluster of differentiation 4
CD66b (CEACAM8)	Carcinoembryonic antigen-related cell adhesion molecule 8
CD69	Cluster of Differentiation 69
CD80 (B7-1)	Cluster of Differentiation 80 (B7, type I)
CD86 (B7-2)	Cluster of Differentiation 86 (B7, type 2)
CD8a	Cluster of Differentiation 8a
Cdkn1a	Cyclin-dependent kinase inhibitor 1A (p21, Cip1)
Csf1 (M-CSF)	Colony Stimulating Factor 1 (Macrophage Colony Stimulating Factor)
CXCL10 (IP10)	C-X-C motif chemokine ligand 10 (Interferon gamma-induced protein 10)
CXCL2 (MIP-2α)	C-X-C motif chemokine ligand 2 (Macrophage Inflammatory Protein 2-Alpha)
CXCL9 (MIG)	C-X-C motif chemokine ligand 9 (Monokine induced by gamma interferon)

(*Continued on next page*)

Table 1. *Continued*

Marker/Gene ID	Description
Cyp1a2	Cytochrome P450, family 1, subfamily A, polypeptide 2
Cyp1b1	Cytochrome P450, family 1, subfamily B, polypeptide 1
Eef1g	Eukaryotic translation elongation factor 1 gamma
Fasn	Fatty acid synthase
Fcer2a (CD23)	Fc Epsilon Receptor II
Fcgr1	High affinity immunoglobulin gamma Fc receptor I
Fmo1	Flavin containing monooxygenase 1
FoxP3	Forkhead box P3
Fpr1	Formyl peptide receptor 1
G6pd	Glucose-6-phosphate dehydrogenase
Gadd45a	Growth arrest and DNA-damage-inducible, alpha
Gapdh	Glyceraldehyde-3-phosphate dehydrogenase
GBP2	Interferon-induced guanylate-binding protein 2
GBP3	Interferon-induced guanylate-binding protein 3
GBP4	Interferon-induced guanylate-binding protein 4
GBP5	Interferon-induced guanylate-binding protein 5
GBP6	Interferon-induced guanylate-binding protein 6
GBP7	Interferon-induced guanylate-binding protein 7
Gclc	Glutamate-cysteine ligase, catalytic subunit
GM-CSF	Granulocyte-macrophage colony-stimulating factor
Gpx1	Glutathione peroxidase 1
Gsr	Glutathione reductase
Havcr2 (Tim-3)	Hepatitis A Virus Cellular Receptor 2 (T cell Immunoglobulin Mucin Domain 3)
Hmox1	Heme oxygenase 1
Hprt	Hypoxanthine phosphoribosyltransferase 1
Icam1	Intercellular adhesion molecule 1
Icam1 (CD54)	Intercellular Adhesion Molecule 1
IFN-a	Interferon alpha
IFN-γ (*Ifng*)	Interferon gamma
IL-10 (*Il10*)	Interleukin 10
IL-4	Interleukin 4
IL-6 (*Il6*)	Interleukin 6
Il12rb1	Interleukin 12 receptor subunit beta 1
Il12rb2	Interleukin 12 receptor subunit beta 2
IL18	Interleukin 18
Il1b	Interleukin 1 Beta
Il1r2 (CD121b)	Interleukin 1 Receptor Type 2
Il1rn	Interleukin 1 Receptor Antagonist
iNOS (*Nos2*)	Inducible nitric oxide synthase (Nitric oxide synthase 2)
IRF1	Interferon regulatory factor 1
IRF4	Interferon regulatory factor 4
IRF7	Interferon regulatory factor 7
Jak1	Janus Kinase 1
Ki67 (*Mki67*)	Antigen KI-67 (Marker of Proliferation Ki-67)
Lmnb1	Lamin B1

(*Continued on next page*)

Table 1. *Continued*

Marker/Gene ID	Description
Lox-1	Lectin-Like Oxidized Low-Density Lipoprotein Receptor 1
Lpl	Lipoprotein lipase
Ly6C (*Ly6c1*)	Lymphocyte antigen 6 complex (Lymphocyte antigen 6 complex, locus C1)
Ly6G (*Ly6g*)	Lymphocyte antigen 6 complex, locus G
MHC-II	Major histocompatibility complex class II
Mt2	Metallothionein 2A
Nqo1	NAD(P)H dehydrogenase, quinone 1
Oas1	2′-5′-Oligoadenylate Synthetase 1A
Oas1g	2′-5′-Oligoadenylate Synthetase 1G
Oasl2	2′-5′-Oligoadenylate synthetase-like 2
Polr1b	RNA polymerase I subunit B
Polr2a	RNA polymerase II subunit A
Ppara	Peroxisome proliferator-activated receptor alpha
Psme2	Proteasome activator subunit 2
Ptafr	Platelet Activating Factor Receptor
Ptgs2 (COX-2)	Prostaglandin-Endoperoxide Synthase 2 (Cyclooxygenase 2)
Rb1	Retinoblastoma 1
Rbp1	Retinol binding protein 1, cellular
Rpl19	Ribosomal protein L19
Sdha	Succinate dehydrogenase complex flavoprotein subunit A
Serpine1	Serpin peptidase inhibitor, clade E (nexin, plasminogen activator inhibitor type 1), member 1
Socs1	Suppressor of cytokine signaling 1
Socs3	Suppressor of cytokine signaling 3
Srebf1	Sterol regulatory element binding transcription factor 1
Stat1	Signal transducer and activator of transcription 1
Stat2	Signal transducer and activator of transcription 2
Stat3	Signal transducer and activator of transcription 3
Stat4	Signal transducer and activator of transcription 4
Stat5a	Signal transducer and activator of transcription 5A
Thrsp	Thyroid Hormone Responsive
Tnf (TNF-α)	Tumor necrosis factor (alpha)
Tnfrsf1a	TNF Receptor Superfamily Member 1A
Tnfrsf1b	TNF Receptor Superfamily Member 1B
Txnrd1	Thioredoxin reductase 1
Tyk2	Tyrosine Kinase 2
VEGF	Vascular endothelial growth factor

Neutrophils were then analyzed for expression of iNOS, Arg-1, PD-L1, CD66b, CD80, and MHC-II (Figures 1D–1I). Within males, the % iNOS+ neutrophils were significantly increased ($p < 0.0001$) for the 10 mg IL12ns group over all other experimental groups at T2, T4, and T6 (exception - T2 and T6, versus 0.1 mg IL12ns group). A significant ($p < 0.0001$) or trending increase in this cellular population continued for 10 mg IL12ns over all other experimental groups at T7. This finding was also consistent within female mice, albeit only at T4 and T6 (Figure 1D). Analysis revealed a significant increase ($p < 0.0001$) in % Arg-1+ neutrophils for the 10 mg IL12ns group in comparison to all other experimental groups at T2 and T4 within male mice. A similar significant increase ($p < 0.001$) was present in female mice, albeit only at T4 (Figure 1E). Importantly, at T3, T4, T5, and T7, there were significant increases ($p < 0.0001$) within the % PD-L1+ neutrophil population for the MTD group versus all other experimental groups in males, with a significant increase also evident at T2 within females. While still significantly elevated, levels of this cellular population drop from a peak (~20% of all cells) at T2 to less than 5% of all cells at T7 (Figure 1F). Analysis of % CD66b+ neutrophils showed no differences across experimental groups at all timepoints examined (Figure 1G). However, the % $CD80^{+}$ neutrophils displayed a significant increase ($p < 0.0001$) in the 10 mg IL12ns group at T2 and T4, with similar findings persisting within female

mice (Figure 1H). Finally, a significant (female, $p < 0.0001$) or trending (male) increase in % MHC-II+ neutrophils was evident for the 10 mg IL12ns group over all other experimental groups at T5, with additional trending increases also evident at T7 for female mice (Figure 1I). Overall, it appears that while the MTD strategy initiates the release of dysfunctional and immunosuppressive neutrophils positive for PD-L1,[32] IL12ns drives transient increases in phagocytic, inflammatory neutrophils capable of initiating pro-inflammatory immune responses.[33]

While there were limited effects of either IL12ns or MTD on monocytic-like (M)-MDSCs (File S1), analysis of PMN-MDSCs revealed potential hyper-sensitivity to the bolus MTD strategy. First, both male and female mice displayed transient changes in the overall PMN-MDSC population across the timepoints examined (Figure 1J). However, when analyzing the PMN-MDSC population for iNOS, Arg-1, PD-L1, CD66b, CD80, and MHC-II expression (Figures 1K–1P), distinct differences became apparent. First, a significant increase ($p < 0.0001$) in % iNOS+ PMN-MDSCs was evident for the MTD group over 10 mg IL12ns and 0.1 mg IL12 ns at T2 and T5, respectively. However, at T7, there were significant increases ($p < 0.0001$) within the 10 mg IL12ns over 0.001 mg IL12ns, MTD, and saline control groups. A similar trend was also evident within females, albeit with additional significant increases ($p < 0.0001$) in MTD versus saline control at T3 (Figure 1K). Further, while there was a significant increase of % Arg-1+ PMN-MDSCs at T2 for the MTD group over 10 mg IL12ns, there was again an eventual shift by T7 resulting in a significant increase ($p < 0.0001$) of this population within the 10 mg IL12ns group over 0.001 mg IL12ns, MTD, and saline control groups for both males and females (Figure 1L). Most importantly, there were significant increases ($p < 0.0001$) in % PD-L1+ PMN-MDSCs for the MTD group versus all experimental groups from T2 through T7. Similar findings were apparent in female mice, with significant increases ($p < 0.0001$) in this population evident at T3, T4, T5, and T7 for the MTD group (Figure 1M). Further, the % CD66b+ PMN-MDSCs displayed a significant increase ($p < 0.0001$) within the male MTD group over 10 mg, 0.1 mg IL12ns, and saline control groups at T2, T4, and T5, with a trending increase over 0.001 mg IL12ns evident at the same timepoints. This finding was also apparent for female mice at T2 through T5, revealing the generation of an activated PMN-MDSC population with the MTD[34] (Figure 1N). Similarly, within female mice, there was a significant increase ($p < 0.0001$) in % $CD80^+$ PMN-MDSCs for the MTD group when compared to 10, 0.1 mg IL12ns as well as saline control groups at T3 and T5. While an increase was also evident in male MTD mice, the % $CD80^+$ PMN-MDSCs was only significantly increased for the MTD group in comparison to 10 mg IL12 ns at T4 (Figure 1O). Finally, there was a significant increase ($p < 0.0001$) in the % MHC-II+ PMN-MDSCs for the MTD group at T7 in both male and female mice (Figure 1P). This expression is likely a maladaptive response to IL-12 overstimulation.[35] Ultimately, the MTD strategy drives an increase in % PD-L1+, CD66b+, and MHC-II+ PMN-MDSCs. Increased antigen presentation alongside immune checkpoint inhibitor expression on PMN-MDSCs was previously associated with T cell suppression through heightened T-cell-PMN-MDSC interactions,[35] a likely maladaptive effect of IL-12 overstimulation with the MTD strategy.

Spectral flow cytometric analysis also revealed transient differences in T-lymphocyte ($CD4^+$ T helper, $CD8^+$ Cytotoxic, and FoxP3+ T regulatory) populations between experimental groups. The % $CD19^+$ B-lymphocytes experienced significant declines at T2, T4, and T6 within the 10 mg IL12ns group. Natural Killer (NK) cells experienced initial proliferation, as evidenced by increases in % Ki67+ NK cells within the MTD group at T3. However, this proliferative capacity was not sustained, evidenced by declines in NK cells in both MTD and 10 mg IL12ns dosing strategies over time (File S1). This early proliferation (evidenced by Ki67 positivity), followed by subsequent declines in immune cell populations (particularly NK cells), may indicate pathological overstimulation and inflammatory cell death with the MTD strategy.

Bulk PBMC RNA-seq analysis – Myeloid and lymphoid gene expression

Total RNA isolated from PBMCs was evaluated using next-generation bulk RNA-sequencing (RNA-seq). There were, on average, 24.6 ± 14.5 million reads per sample with a $91.9 \pm 0.02\%$ mapping rate to the murine mm10 genome. Samples also displayed adequate clustering at each timepoint by principal component analysis (PCA) (data not shown). Following the generation of reads per kilobase of transcript per million reads mapped (RPKM) matrices, gene expression differences between experimental groups were analyzed. Our group first evaluated correlating genes of the myeloid flow cytometric panel. Importantly, there was a significant increase ($p < 0.01$) in *PD-L1* expression for the male MTD group versus all other experimental groups at T2 (exception – 10 and 0.1 mg IL12ns), T3, T4 (exception – 10 mg IL12ns), T5, T6, and T7. A similar trend was also apparent in female mice, with a significant increase evident for the MTD group versus all experimental groups at T2 through T6 (Figure S2F). Overall, these data corroborated previous flow cytometric findings which indicated an increase in myeloid lineage cells in peripheral blood with 10 mg IL12ns dosing (*Itgam, Ly6g, Nos2*). Evidence of IFN-γ-driven peripheral immune activation with MTD (*PD-L1*) was also evident (Figures S2A–S2F and File S2).

Differences within lymphoid-related gene expression, including but not limited to *CD4*, *CD8a*, *Foxp3*, *CD19*, and *Ncr1* (NKp46), were also examined. These data also provided further support to the previous flow cytometric analysis which suggested that elevated IL-12 dosing (10 mg IL12ns and MTD) had limited effect on peripheral T-lymphocyte cell populations. However, these dosing strategies were further associated with decreases in $CD19^+$ B-lymphocytes (mainly 10 mg IL12ns) and initial yet unstainable increases in NK cells (both 10 mg IL12ns and MTD) (Figures S2G–S2K). Further analysis of lymphoid immune exhaustion genes including *CTLA-4*, *Lag3*, and hepatitis A virus cellular receptor 2 (*Havcr2*, Tim-3) revealed increased gene expression with MTD (Figures S2L–S2N and File S2). Importantly, there were significant increases ($p < 0.01$) in *Lag3* gene expression for the MTD group versus both 0.1 mg IL12ns and saline control at T3, possibly indicating early signs of immune exhaustion. This finding was apparent, however, only trending in the female MTD group at both T2 and T3 (Figure S2M). There were also significant ($p < 0.01$) or trending increases in *Havcr2* expression within the MTD group at T2 (versus 10 mg IL12ns and saline), T3 (versus 0.1 mg IL12ns and saline), and T6 (versus all other groups). This result was also observed in female MTD mice, albeit only trending ($p = 0.025$) at T4 versus the 10 mg IL12ns group (Figure S2N). Overall, bulk PBMC RNA-seq analysis conveys prominent immunological changes for the lymphoid functional markers examined and suggests the generation of a hyporesponsive immune signature in peripheral lymphoid cells with the MTD strategy.

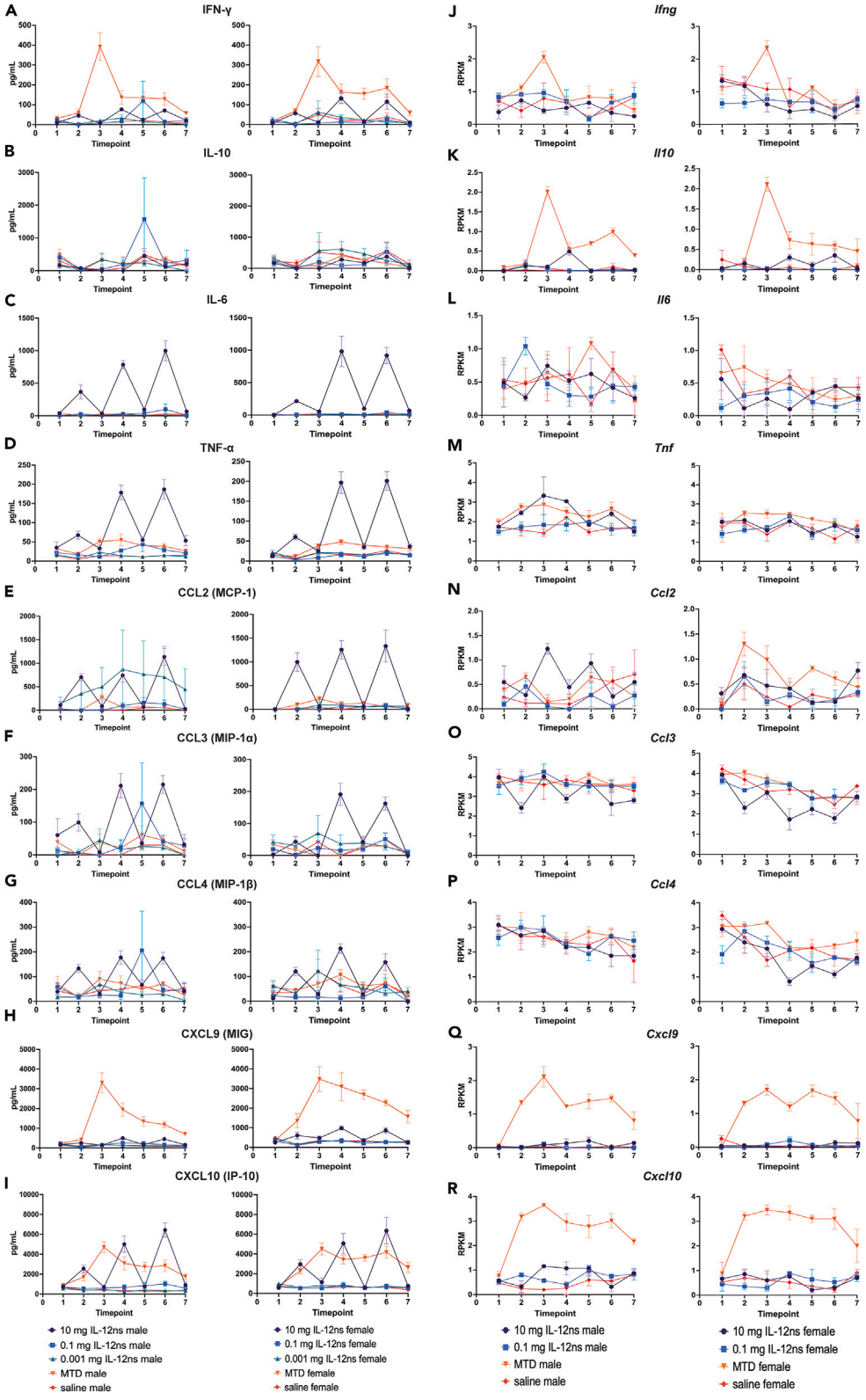
A
IFN-γ
B
IL-10
C
IL-6
D
TNF-α
E
CCL2 (MCP-1)
F
CCL3 (MIP-1α)
G
CCL4 (MIP-1β)
H
CXCL9 (MIG)
I
CXCL10 (IP-10)
pg/mL
Timepoint
J
Ifng
K
Il10
L
Il6
M
Tnf
N
Ccl2
O
Ccl3
P
Ccl4
Q
Cxcl9
R
Cxcl10
RPKM
10 mg IL-12ns male
0.1 mg IL-12ns male
0.001 mg IL-12ns male
MTD male
saline male
10 mg IL-12ns female
0.1 mg IL-12ns female
0.001 mg IL-12ns female
MTD female
saline female

Figure 2. Peripheral blood plasma and bulk PBMC RNA-seq analysis indicated differential response to IL-12 dosing strategies

(A–R) Plasma was isolated at each serial blood sampling timepoint [baseline (T1, n = 7 for MTD male), 12-h (T2), day 4 (T3, n = 7 for 10 mg IL12ns male, MTD male, saline male, 0.1 mg IL12ns female), day 8 (T4, n = 7 for 0.001 mg IL12ns male, saline male, 0.1 mg IL12ns female), day 11 (T5, n = 7 for saline male and 10 mg female), day 15 (T6, n = 7 for saline male and 10 mg female), and day 18 (T7, n = 6 for saline male, n = 7 for 10 mg female)]. Plasma cytokines including IFN-γ (A), IL-10 (B), IL-6 (C), and TNF-α (D), as well as chemokines CCL2 (MCP-1) (E), CCL3 (MIP-1α) (F), CCL4 (MIP-1β) (G), CXCL9 (MIG) (H), and CXCL10 (IP-10) (I), were quantified (pg/mL) using the BioLegend LEGENDplex Cytokine Release Syndrome Panel (male mice – left, female mice – right). Unless indicated above, an n = 8 mice per group per sex were included in the analysis at each timepoint. Bulk PBMC RNA-seq was also utilized to evaluate gene expression of *Ifng* (J), *Il10* (K), *Il6* (L), and *Tnf* (M), *Ccl2* (N), *Ccl3* (O), *Ccl4* (P), *Cxcl9* (Q), and *Cxcl10* (R) (male mice – left, female mice – right). An n = 3 mice per group per sex were included in the bulk PBMC RNA-seq analysis at each timepoint. Where visible, error bars represent standard error of the mean (SE). For visual clarity, findings from statistical analyses can be found in Files S2 and S3. The x axis represents the timepoint of blood collection while the y axis indicates either concentration (pg/mL) or gene expression (reads per kilobase of exon model per million mapped - RPKM).

Plasma proteomic analysis – Cytokines

Distinct differences in the plasma cytokines IFN-γ, IL-10, IL-6, and TNF-α were also measured (Figures 2A–2D). There were significant increases ($p < 0.0001$) in IFN-γ concentration (pg/mL) for the male MTD group at T3 versus all other groups, with trending increases versus 0.1 mg, 0.001 mg IL12ns, and saline at T4. There was also a significant increase ($p < 0.0001$) over 0.1 and 0.001 mg IL12ns as well as saline control groups at T6. Most importantly, the increase at T2 was not sustained, as evidenced by an over 4-fold decrease in IFN-γ levels by T7. In contrast, the 10 mg IL12ns group maintained its peak IFN-γ levels with repeated dosing at IL12ns dosing timepoints T2, T4, and T6. Interestingly, the female 10 mg IL12ns group also experienced significant (versus 0.1 mg IL12ns, $p < 0.0001$) or trending (versus 0.001 mg IL12ns, $p = 0.0001$) increases in IFN-γ levels at T2 (Figure 2A). There were no significant differences in IL-10 concentration (pg/mL) measured amongst groups at all sampling timepoints (Figure 2B). This finding is likely related to the highly transient nature of IL-10 and difficulty quantifying this cytokine within plasma/serum samples.[36,37]

Plasma proteomic analysis also revealed a significant increase ($p < 0.0001$) of IL-6 within male 10 mg IL12ns versus all other experimental groups at T2, T4, T6, and T7 (exception – only trending increase versus 0.1 mg IL12 ns at T2 and versus saline control at T7). A similar finding was also evident in female mice, however, the increase for the 10 mg IL12ns group at T7 was merely trending versus all other groups. Additionally, there was a significant increase ($p < 0.0001$) in IL-6 concentration in the female 10 mg IL12ns group when compared to all other experimental groups at T5 (Figure 2C). Similarly, a significant increase ($p < 0.0001$) in TNF-α concentration was evident in the 10 mg IL12ns group versus all other experimental groups at T2, T4, and T6, further indicating the activation of acute inflammatory responses with 10 mg IL12ns dosing. Additional trending and significant increases for the 10 mg IL12ns and MTD groups were also measured versus all other experimental groups at T5 (Figure 2D, File S3). This observation suggests that increased TNF-α could be, in part, associated with large-dose IL-12 therapy.[38]

Plasma proteomic analysis – Chemokines

Plasma samples were also analyzed for concentration of circulating pro-inflammatory chemokines CCL2 (MCP-1), CCL3 (MIP-1α), CCL4 (MIP-1β), CXCL9 (MIG), and CXCL10 (IP-10) (Figures 2E–2I). A significant increase ($p < 0.0001$) in CCL2 concentration was measured within the female 10 mg IL12ns group versus all other experimental groups at T2, T4, and T6. While not significant in males, comparable increases were also evident (Figure 2E). Similarly, there were significant increases ($p < 0.0001$) in CCL3 concentration for the male 10 mg IL12ns group when compared to all other experimental groups at T2, T4, and T6 (again, timepoints associated with IL12ns dosing). In females, a similar significant increase ($p < 0.0001$) was evident at T4 and T6 (Figure 2F). Significant increases ($p < 0.0001$) in CCL4 concentration were also measured within the male 10 mg IL12ns group versus all other experimental groups at T2 and T6 (exception, only trending increase versus MTD at T6). Similar findings were again evident in female mice, albeit at T2 and T4 (Figure 2G).

Additionally, CXCL9 concentration (pg/mL) was significantly increased ($p < 0.0001$) for male MTD group versus all other groups from T3 through T7, with additional significant (versus 0.1 and 0.001 mg IL12ns, $p < 0.0001$) and trending (versus saline control, $p = 0.0003$) increases evident at T2. The peak in CXCL9 at T3 was not sustained with MTD, with a near 3-fold decrease toward baseline levels by T7. These findings were consistent in female mice and may indicate exhaustive IL-12 stimulation within peripheral blood (Figure 2H). Furthermore, significant increases ($p < 0.0001$) in CXCL10 were evident in both the male MTD and 10 mg IL12ns groups versus both 0.1, 0.001 mg IL12ns and saline control groups at T2. At T3 and T5, there was a significant increase ($p < 0.0001$) in CXCL10 concentration for the MTD versus all other experimental groups. However, at T4 and T6, significant ($p < 0.0001$) or trending increases in the 10 mg IL12ns group emerged. While these findings were also demonstrated in the female groups, there remained a significant increase ($p < 0.0001$) in CXCL10 for the MTD group compared to all other experimental groups at T7 (exception – trending increase versus 10 mg IL12ns) (Figure 2I and File S3).

Bulk PBMC RNA-seq analysis – Cytokine and chemokine gene expression

Circulating PBMCs were also analyzed for expression of the previously identified cytokine-related genes *Ifng*, *Il10*, *Il6*, and *Tnf* (Figures 2J–2M). Within males, there was a significant (versus 10 mg IL12ns) or trending (versus saline control) increase in *Ifng* gene expression in the MTD group at T3. Similarly, the female MTD group displayed a significant increase ($p < 0.01$) in *Ifng* gene expression over all other groups at this same timepoint (Figure 2J). This result correlated with a significant increase ($p < 0.01$) in *Il10* gene expression for both the male and female MTD groups versus all other groups at T3. This significant increase in *Il10* expression was then maintained at T4 (trending versus 0.1 mg IL12ns

and saline), T5, T6, and T7 for the male MTD group in comparison to all other groups. A similar finding was evident in females, with trending increases in *Il10* expression evident at T4 and T6 for the MTD group in comparison to both 0.1 mg IL12ns and saline control groups (Figure 2K). Furthermore, analysis revealed a trending increase in *Il6* gene expression for the MTD group versus both the 0.1 mg IL12ns and saline control groups at T5 in males (Figure 2L). Additionally, *Tnf* analysis in male mice revealed trending increases at T2 (MTD versus saline control) and T4 (10 mg versus 0.1 mg IL12ns) for both MTD and 10 mg IL12ns groups, respectively. Similar findings were evident in females, where a trending increase in *Il6* expression was evident for the MTD group in comparison to the 0.1 mg IL12ns group at T2 (Figure 2M). Importantly, these gene expression results for both *Il6* and *Tnf* contrast with the proteomic cytokine analysis previously highlighted. While circulating levels of both IL-6 and TNF-α are increased in the 10 mg IL12ns group, RNA isolated from PBMCs suggests minimal gene expression changes in circulating immune cells.

Analysis of chemokine-related genes *Ccl2*, *Ccl3*, *Ccl4*, *Cxcl9*, and *Cxcl10* also revealed important trends (Figures 2N–2R). Within males, a significant increase ($p < 0.01$) in *Ccl2* gene expression was evident for the 10 mg IL12ns group versus all other groups at T3. Analysis in females revealed significant ($p < 0.01$, versus 10 and 0.1 mg IL12ns) or trending (versus saline control) increases in *Ccl2* expression within the MTD group at T5 (Figure 2N). Additionally, a trending decrease in *Ccl3* expression was measured within the male 10 mg IL12ns group at T4 versus saline control. Similarly, in females, there were significant (T2) or trending (T4) decreases in *Ccl3* gene expression for the 10 mg IL12ns group in comparison to all other groups (exception – no decrease versus 0.1 mg IL12 ns at T2) (Figure 2O). While there were no differences in *Ccl4* gene expression amongst all experimental groups in males, there were trending or significant ($p < 0.01$) increases in *Ccl4* expression for the female MTD group versus 10 mg IL12ns (T4, T6) and saline control (T3) groups (Figure 2P). Importantly, in both males and females, there was a significant increase ($p < 0.01$) in *Cxcl9* gene expression within the MTD group versus all other groups at T2 through T6, with a trending increase also evident for the male MTD group at T7 (Figure 2Q). Similarly, *Cxcl10* gene expression in males revealed a significant increase ($p < 0.01$) in gene expression for the MTD group versus all other groups at T2 through T7. Additional significant (versus 0.1 mg IL12ns) or trending (versus saline) increases for the 10 mg IL12ns group were evident at T3. For females, a significant increase ($p < 0.01$) in *Cxcl10* gene expression was also evident for the MTD group versus all other experimental groups at T2 through T6 (Figure 2R and File S2). Importantly, while CXCL10 plasma levels were indeed elevated with IL12ns treatment, those circulating immune cells ultimately lack *Cxcl10* gene expression. This finding may suggest the initiation of tissue-resident pro-inflammatory signal transduction as opposed to stimulation within the peripheral blood (as seen with the MTD strategy).

Bulk PBMC RNA-seq analysis – GSEA

A targeted gene set enrichment analysis (GSEA) was performed on the Reactome[39] gene sets Interferon gamma signaling (IFNG),[40] Interleukin-12 signaling (IL12),[41] Interleukin-10 signaling (IL10),[42] and Tumor necrosis factor (TNF) signaling.[43] For simplicity, this assessment was conducted at the timepoint of maximal gene expression differences between treatment groups and saline control (T3). For both male and female MTD groups, GSEA Reactome analysis revealed significant upregulation of the IFNG, IL12, and IL10 signaling pathways in comparison to matched-sex saline controls (Figure 3). While neither 10 mg or 0.1 mg IL12ns groups displayed a significant increase in IFNG, IL12, or TNF pathways (exception – trending increase for IFNG Reactome in 10 mg IL12ns female), both showed significant upregulation of the IL10 signaling Reactome at T3 versus the saline control (Figure 3A). A similar relationship was also apparent in female mice, albeit only within the 0.1 mg IL12ns dosing group (Figure 3B). Further analysis of the individual genes that compose the IL10 signaling Reactome is ultimately required to discern differences in this increase between experimental groups. No experimental group displayed alterations in the TNF signaling Reactome at this timepoint. An unbiased GSEA using both Hallmark[44] (Table S1) and Reactome[39] gene sets (Table S2) further supported the modulation of these isolated pathways. Interestingly, both male and female MTD groups displayed statistically significant upregulation of the Reactome signature pyroptosis, or caspase-1 mediated inflammatory cell death[45–48] ($q = 0.0498$ and 0.0225, respectively, Table S2). These data further suggest overt immunological toxicity with the bolus MTD strategy even at early dosing timepoints (T3). The core enrichment genes identified from these GSEA Reactome analyses (Figure S3) were then assessed for expression changes at all peripheral blood sampling timepoints T1-T7.

Bulk PBMC RNA-seq analysis – IFNG signaling reactome

In addition to the previously highlighted *Ifng* (Figure 2J), RPKMs for individual core enrichment genes within the IFNG signaling reactome[40] were also analyzed (Figures 4A–4K). To begin, significant increases in *Fcgr1* expression were evident in the male MTD group versus all other groups at T3 through T5 (exception – 10 mg IL12ns), T6, and T7. Similar yet less pronounced increases were evident in the female MTD group (Figure 4A). Furthermore, analysis of the interferon-induced *Gbp2*, *Gbp3*, *Gbp5*, and *Gbp7* revealed similar expression changes for males and females (Figures 4B–4E). Overall, the MTD group exhibited significant ($p < 0.01$) or trending increases in *Gbp* expression versus all other experimental groups (with few exceptions) from T3 through T7, with additional significant increases evident at T2 (*Gbp5*, *Gbp7*). Interestingly, the 10 mg IL12ns group displayed a significant increase in *Gbp2* expression at T2 (versus saline), T3, T4, T6, and T7 (versus 0.1 mg IL12ns and saline) (Figure 4B). For *Gbp7*, the 10 mg IL12ns group also exhibited significant or trending increases at T2 (versus saline), T4, T5 (versus 0.1 mg IL12ns and saline), T6 (versus saline), and T7 (versus 0.1 mg IL12ns and saline) (Figure 4E).

Additionally, analysis revealed significant increases ($p < 0.01$) in *Irf1* gene expression for the male MTD group at T2, T3, T4, T5, and T6 versus all groups, as well as at T7 versus both the 0.1 mg IL12ns and saline control groups. Significant or trending increases were also evident for the 10 mg IL12ns group at T2, T3, and T4 (versus 0.1 mg IL12ns and saline control), as well as T6 and T7 (versus saline control) (Figure 4F). Further, *Irf7* expression displayed significant ($p < 0.01$) or trending increases within both male and female MTD groups in comparison to all

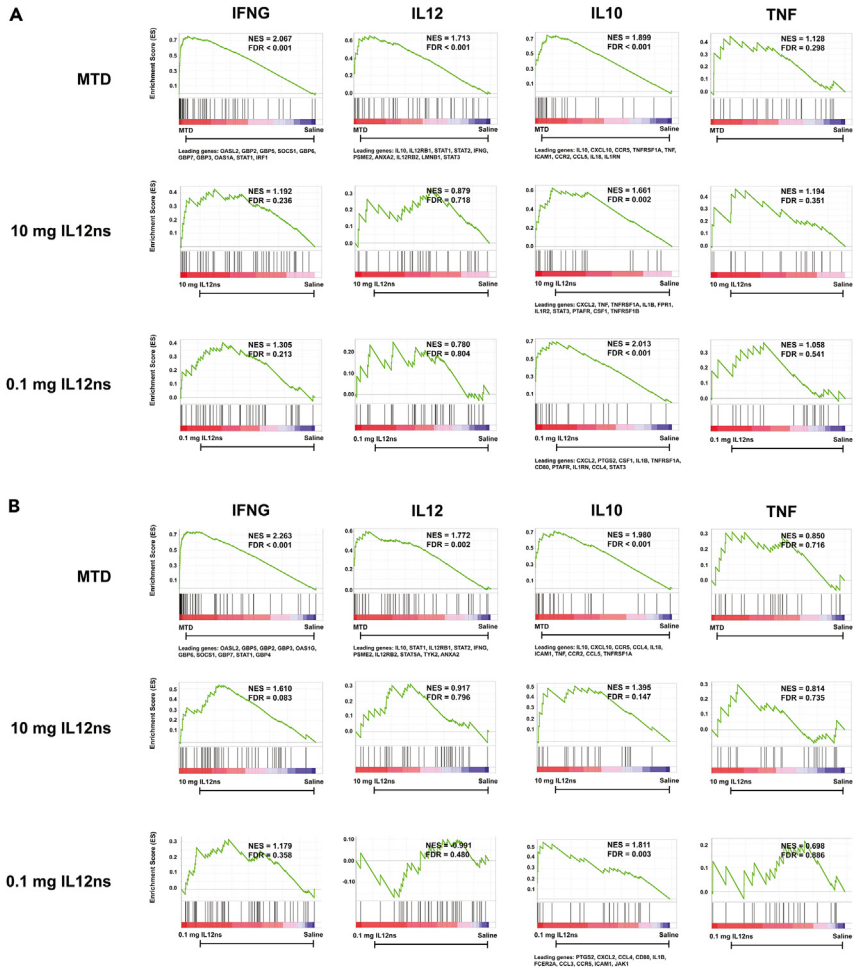

Figure 3. GSEA indicated aberrant peripheral immune stimulation with the MTD strategy

Gene set enrichment analysis (GSEA) of four Reactome[39] gene sets including Interleukin-12 signaling,[41] Interferon gamma signaling,[40] Interleukin-10 signaling,[42] and TNF signaling[43] were analyzed for male (A) and female (B) experimental groups at timepoint 3 (T3). Both the normalized enrichment score (NES) and false discovery rate (FDR) are presented on each enrichment score (ES) graph, separated by Reactome pathway (top) and experimental group (left). An n = 3 mice per group per sex were included in this GSEA. Leading genes for each Reactome pathway (presented below each associated graph) are considered statistically significant (FDR q-value <0.05).

other experimental groups from T2 through T7 (Figure 4G). Similarly, *Irf9* expression was significantly increased within the male MTD group in comparison to the saline control group at T2, T3, T6, and T7. Additional significant increases ($p < 0.01$) were also evident within the male 10 mg IL12ns group versus saline at T2, T3, T4, with trending increases evident at T3 (versus 0.1 mg IL12ns), T6, and T7 (versus saline). Overall, similar findings were also apparent for female experimental groups (Figure 4H).

Both male and female MTD groups also exhibited significant increases in *Oasl2* gene expression at T2 through T7 versus all other experimental groups. Additional trending or significant increases were apparent in the male 10 mg IL12ns group at T2 (versus saline), T3, T4, T5, and T7 (versus saline and 0.1 mg IL12ns) (Figure 4I). Importantly, expression of the signal transducer of the IFNG pathway, *Stat1*,[49] was significantly upregulated at T2 through T6 for the male MTD group versus all other groups (exception – not in comparison to 10 mg IL12 ns at T4). A significant or trending increase in *Stat1* gene expression was also apparent within the 10 mg IL12ns group at T2, T3, T4, T6, and T7. Similar trends were evident within the female MTD and 10 mg IL12ns groups, further suggesting IFNG signaling activation in these groups (Figure 4J). Importantly, *Socs1* was significantly upregulated in the male MTD group at T2 (versus 0.1 mg IL12ns and saline), T3 (versus all other groups), T4 (versus 0.1 mg IL12ns and saline), as well as T5 and T6 (versus all other groups). Similar trends persist within female MTD mice, with a significant increase ($p < 0.01$) in *Socs1* gene expression evident at T2, T3, T5, and T6 (exception 10 mg IL12ns) versus all other groups. Additional significant or trending increases within the 10 mg or 0.1 mg IL12ns group versus saline controls were apparent at early dosing timepoints T3 (both groups) and T4 (10 mg IL12ns) within males, as well as T2 (10 mg Il12ns) within females (Figure 4K). The lack of markedly increased *Socs1* expression at later timepoints with IL12ns dosing likely suggests a more controlled pro-inflammatory signature within this group (File S2).

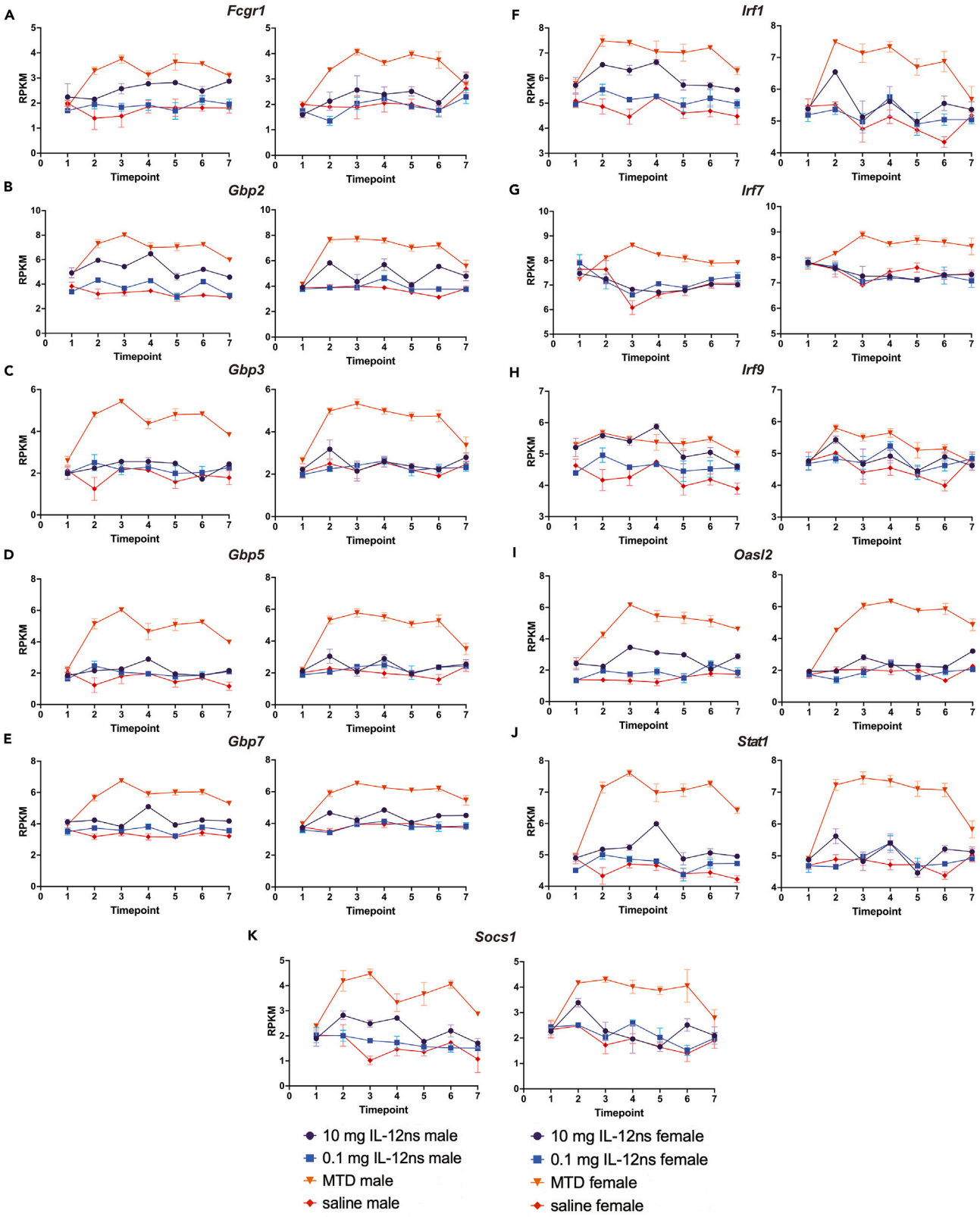
A
Fcgr1
B
Gbp2
C
Gbp3
D
Gbp5
E
Gbp7
F
Irf1
G
Irf7
H
Irf9
I
Oasl2
J
Stat1
K
Socs1
RPKM
Timepoint
10 mg IL-12ns male
0.1 mg IL-12ns male
MTD male
saline male
10 mg IL-12ns female
0.1 mg IL-12ns female
MTD female
saline female

Figure 4. Core enrichment gene analysis of the IFNG Reactome supported peripheral immune stimulation and compensatory downregulation with the MTD strategy

(A–K) RPKMs for individual core enrichment genes within the interferon gamma (IFNG) signaling[40] Reactome including *Fcgr1* (A), *Gbp2* (B), *Gbp3* (C), *Gbp5* (D), *Gbp7* (E), *Irf1* (F), *Irf7* (G), *Irf9* (H), *Oasl2* (I), *Stat1* (J), and *Socs1* (K) were analyzed (male mice – left, female mice – right). An n = 3 mice per group per sex were included in the bulk PBMC RNA-seq analysis at each timepoint. Where visible, error bars represent standard error of the mean (SE). For visual clarity, findings from statistical analyses can be found in File S2. The x axis represents the timepoint of blood collection while the y axis indicates gene expression (reads per kilobase of exon model per million mapped - RPKM).

Bulk PBMC RNA-seq analysis – IL12 signaling Reactome

In addition to the previously described *Ifng* (Figure 2J), *Il10* (Figure 2K), and *Stat1* (Figure 4J), RPKMs for individual genes of the Interleukin-12 signaling Reactome[41] were also analyzed (Figures S4A–S4E). Importantly, *Il12rb1* gene expression appeared sensitive to peripheral immune stimulation with bolus IL-12 delivery (MTD). Here, there was a significant increase ($p < 0.01$) in *Il12rb1* gene expression within the male MTD group at T2 (versus saline), T3 (versus 0.1 mg IL12ns, saline), and T5 (versus all other groups), with trending increases evident at T2 versus both 10 and 0.1 mg IL12ns groups, T3 versus 10 mg IL12ns, and T7 versus all other groups. Similar yet less pronounced trends were also evident for female MTD mice (Figure S4A). Analysis of *Stat4* expression indicated possible overstimulation and suppression of IL-12 signaling with elevated IL-12 dosing strategies (10 mg IL12ns, MTD).[50] In females, there were significant decreases ($p < 0.01$) in *Stat4* gene expression within the 10 mg IL12ns group at T4 (versus 0.1 mg IL12ns) and T6 (versus 0.1 mg IL12ns and saline control). This result was accompanied by significant decreases in *Stat4* expression for the female MTD group at T4 and T6 (versus 0.1 mg IL12ns), as well as T7 (versus both 0.1 mg IL12ns and saline control) (Figure S4E). Overall, these data suggest that increased *Il12rb1* expression[51] alongside a compensatory downregulation of *Stat4* expression[52] may indicate peripheral overstimulation with IL-12 delivery (File S2).

Bulk PBMC RNA-seq analysis – IL10 signaling reactome

In addition to the previously described *Il10* (Figure 2K), *Tnf* (Figure 2M), *Ccl4* (Figure 2P), and *Cxcl10* (Figure 2R), RPKMs for core enrichment genes of the Interleukin-10 signaling Reactome[42] were also examined (Figures S4F–S4K). The IFN-γ associated genes of this pathway, including *Il18* (IFN-γ-inducing factor)[53] (Figure S4F), *Icam*[54,55] (Figure S4G), and *Ccr5*[56] (Figure S4H), were more significantly upregulated within the MTD group in comparison to IL12ns, further affirming peripheral immune activation of the IFNG pathway with unencapsulated IL-12 delivery. STAT3 is a crucial regulator at the crossroads of both inflammatory and anti-inflammatory responses.[57] The IL-10/STAT3-mediated anti-inflammatory immune signaling works in opposition of the pro-inflammatory IL-6/STAT3 pathway.[58] Interestingly, in males, *Stat3* gene expression was significantly upregulated within the 10 mg IL12ns group at T2 (versus saline), T3 (versus saline), T4 (versus all other groups), and T7 (versus saline). In females, *Stat3* was significantly upregulated in both the 10 mg IL12ns and MTD groups in comparison to the saline control at T6 (Figure S4I). *Stat3* increases in the 10 mg IL12ns group are likely associated with significant increases in IL-6 plasma cytokine levels[58] at IL12ns dosing timepoints considering the lack of *Il10* expression within this group. Similar gene expression increases were also apparent for *Cxcl2*, an acute inflammatory chemokine[59] (Figure S4J). Significant decreases in *Ptgs2* expression were evident with 10 mg IL12ns dosing (Figure S4K and File S2), suggesting a lack of suppressive PGE_2 production and sustained inflammatory capacity with IL12ns therapy.[60–63] Overall, while the IL10 signaling Reactome was significantly upregulated in both IL12ns and MTD strategies at T3 (Figure 3), the individual core enrichment genes driving this significance are distinctly different. Importantly, significance within the MTD group is driven by expression of compensatory *Il10* and *Ifng*-associated genes. In contrast, genes driving significance within the IL12ns dosing groups are associated with pro-inflammatory signal transduction, however, without compensatory *Il10* gene expression (Figure S3).

Histopathologic analysis

Full necropsy for histopathological analysis by two independent board-certified pathologists and a veterinarian medical doctor was performed at T7 (euthanasia). Representative Hematoxylin and Eosin (H&E) stained sections highlighting differences in portal (liver), cortical (kidney), interstitial (lung), endomyocardial (heart), and stromal (spleen) inflammation amongst both male (Figure 5A) and female (Figure 5E) experimental groups are presented. Additional pathological findings from these analyses can be found in File S4. Quantification of pathological findings into a total pathology, total inflammation, and total necrosis scores revealed striking differences between experimental groups (Figures 5B–5D, and 5F–5H). In males, statistical analysis revealed significant increases in total pathology score for both 10 mg IL12ns and MTD group in comparison to 0.001 mg IL12ns and matched-sex saline control groups (Figure 5B). Additionally, there was a significant increase in total pathology score for the MTD group versus 0.1 mg IL12ns (Figure 5B). In females, both the 10 mg IL12ns and MTD groups exhibited significant increases in total pathology score in comparison to all other experimental groups (Figure 5F). Importantly, in both males and females, there were no differences in total pathologic necrosis measured between experimental groups (Figures 5C and 5G), suggesting these differences were due to histologically determined inflammation. Accordingly, in both males and females, analysis revealed significant increases in total inflammation for the 10 mg IL12ns and MTD groups in comparison to all other experimental groups (Figures 5D and 5H). These results indicate IL12ns can be effectively delivered to healthy BALB/c mice and increase tissue-level inflammatory responses, albeit greatest within the reticuloendothelial system.[64–66] These data also support previous literature which suggests that female BALB/c mice produce heightened pro-inflammatory responses when compared to their male counterparts.[67]

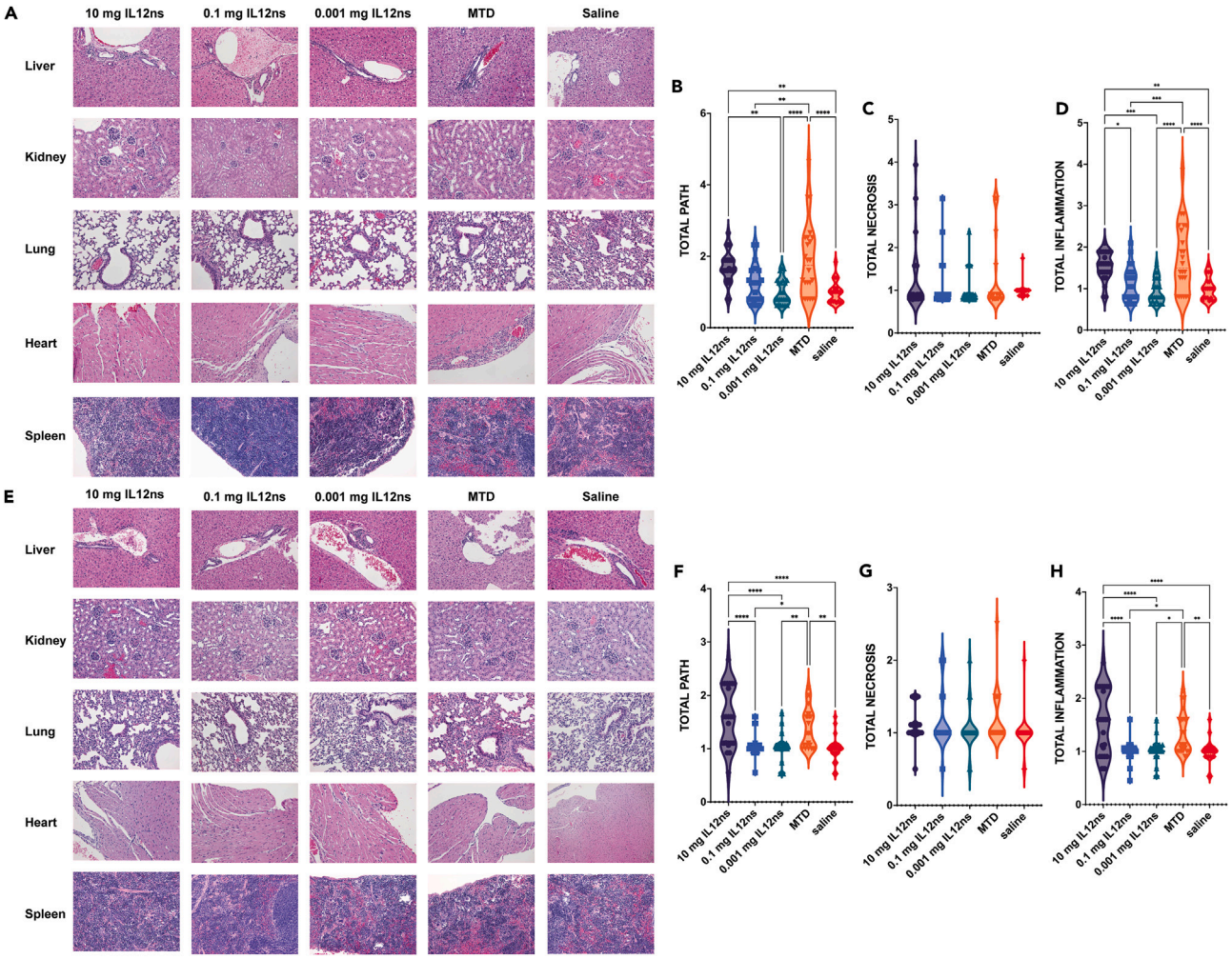

Figure 5. Histopathological assessment revealed increases in total inflammation with MTD and 10 mg IL12ns dosing groups

(A–H) Tissue specimens from male (A–D) and female (E–H) experimental mice were analyzed using a thorough, tissue-specific histopathological guideline. Representative H&E images (A, E) highlight differences in portal (liver), cortical (kidney), interstitial (lung), endomyocardial (heart), and stromal (spleen) inflammation (left). Violin plots display the differences in total pathologic (TOTAL PATH, B, F), total necrosis (C, G), and total inflammation (D, H) scores amongst experimental groups. Results from statistical analysis via a one-way ANOVA are presented (* = $p < 0.05$, ** = $p < 0.01$, *** = $p < 0.001$, **** = $p < 0.0001$).

NanoString nCounter gene expression analysis – Liver

Gene expression profiles of formalin-fixed, paraffin embedded (FFPE) liver specimens harvested at euthanasia (T7) were examined using a 42 gene panel on the NanoString nCounter. Following normalization by housekeeping genes *Eef1g*, *Gapdh*, *Hprt*, *Polr2a*, *Rpl19*, *and Sdha* (both male and female), differentially expressed genes, in comparison to the saline control, were analyzed (Figure 6). Importantly, *Stat3* was significantly increased in both male ($p < 0.01$) and female ($p < 0.05$) 10 mg IL12ns groups, with a trending increase also evident from the female MTD group ($p = 0.0651$) (Figure 6A). This *Stat3* expression is likely associated with pro-inflammatory IL-6 signaling within these specimens.[68] Further, both the 10 mg IL12ns (male – $p < 0.01$, female – $p < 0.05$) and MTD (male and female – $p < 0.01$) groups displayed significant increases in *Ccl2* expression, indicating pro-inflammatory immune cell recruitment[69] (Figure 6B). Both *Cxcl9* and *Cxcl10* displayed increased gene expression in both male and female 10 mg IL12ns and MTD groups, however, their expression was more significantly upregulated in the MTD group (Figures 6C and 6D). When analyzing those genes of the IFNG signaling pathway, interesting trends were revealed. Importantly, *Stat1* gene expression was significantly upregulated in both the 10 mg IL12ns (male – $p < 0.01$) and MTD (male – $p < 0.0001$, female – $p < 0.001$) groups (Figure 6E). Significant or trending increases in *Gbp2* and *Gbp3* expression were also observed for both groups (Figures 6F and 6G). While *Irf1* expression was increased with IL12ns dosing, only the MTD group displayed a significant increase in comparison to the saline control (male – $p < 0.01$, female – $p < 0.001$) (Figure 6H). Furthermore, significant (male) or trending (female) increases in *PD-L1* gene expression was evident for the 10 mg IL12ns group. Analysis of the MTD group, however, revealed significant increases in both *PD-L1* (male and female, $p < 0.01$) and *Lag3* (female, $p < 0.05$) expression (Figures 6I and 6J). Sustained expression of LAG-3 is associated with reduced

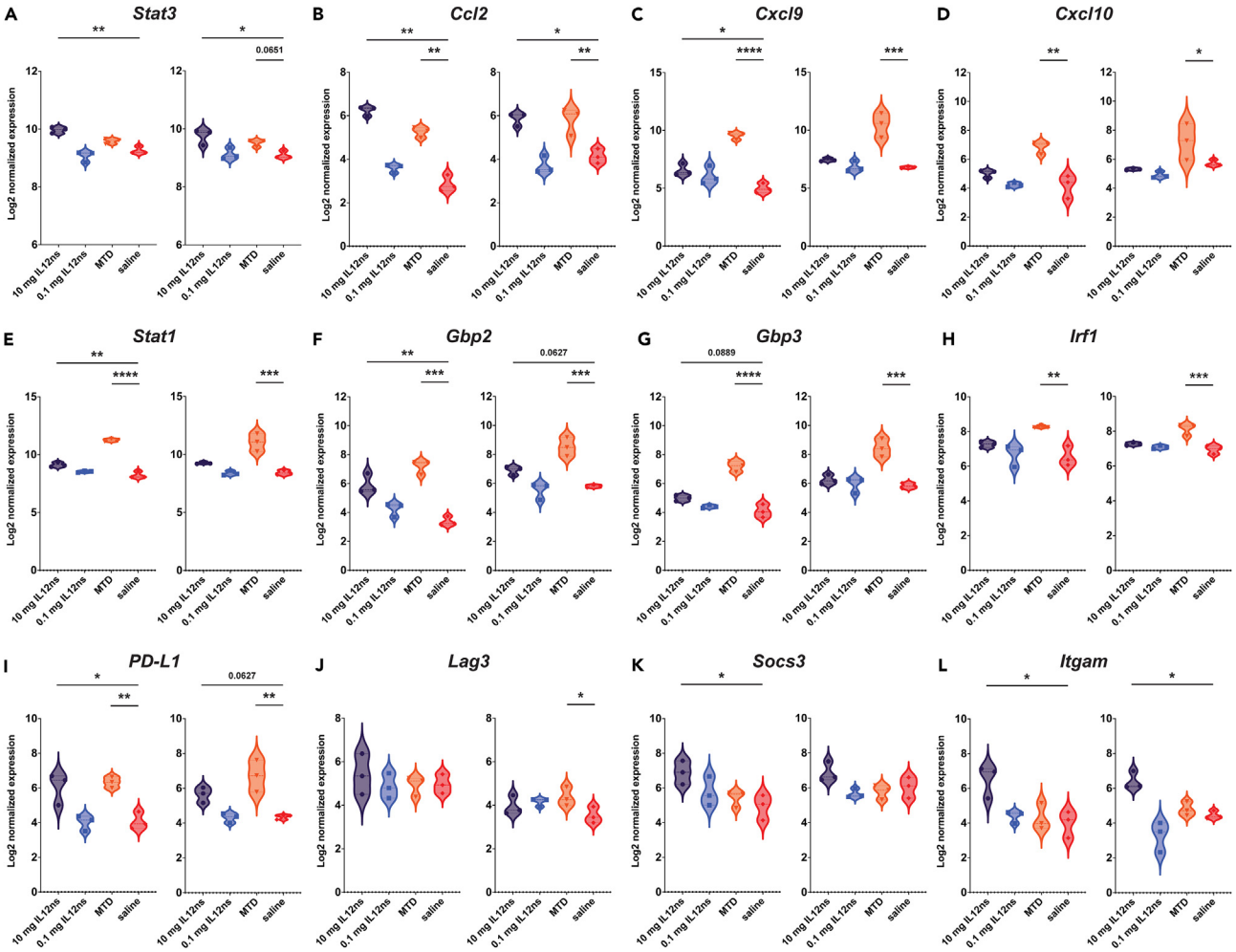

Figure 6. NanoString nCounter analysis reveals sustained pro-inflammatory immune responses with IL12ns dosing in liver specimens collected at euthanasia

(A–L) NanoString nCounter differential gene expression analysis of murine liver specimens revealed significant differences in *Stat3* (A), *Ccl2* (B), *Cxcl9* (C), *Cxcl10* (D), *Stat1* (E), *Gbp2* (F), *Gbp3* (G), *Irf1* (H), *PD-L1* (I), *Lag3* (J), *Socs3* (K), and *Itgam* (L) expression amongst experimental groups in comparison to saline control. Log2 normalized expressions for each experimental group (male mice – left, female mice – right), with an n = 3 mice per group per sex, were analyzed by NanoString nSolver Analysis Software 4.0 and graphed using GraphPad Prism9 (version 9.4.1). Benjamini–Yekutieli adjusted p values were then calculated for each experimental group in comparison to saline controls (* = $p < 0.05$, ** = $p < 0.01$, *** = $p < 0.001$, **** = $p < 0.0001$) as determined by NanoString Advanced Analysis Software.

cytolytic and cytokine-producing functions of infiltrating T cells, while co-expression of LAG-3 and PD-1/PD-L1 exemplifies T cell dysfunction in tumor patients.[70] Significant elevation of both checkpoint molecules with the MTD strategy suggests immunotoxic overstimulation. Finally, the 10 mg IL12ns group displayed significant increases ($p < 0.05$) in both *Socs3* (males) and *Itgam* (males and females) expression (Figures 6K–6L). Upregulation of SOCS3, an integral regulator responsible for maintaining controlled inflammation downstream of both pro-inflammatory STAT1/STAT3 (IL-6) and STAT4 (IL-12) signal transduction,[71,72] suggests healthy inflammatory signaling with IL12ns dosing. Overall, these data support that both IL12ns and MTD strategies drive pro-inflammatory immune responses in murine livers. Importantly, the MTD strategy appears to promote immune exhaustion, as evidenced by increased co-expression of immune checkpoint genes *PD-L1* and *Lag3*. Additionally, a separate drug-induced liver toxicity panel, including the top 30 genes associated with chemical and drug induced liver injury as highlighted in the Comparative Toxicogenomics Database,[73] was also deployed on both male and female liver specimens. NanoString nCounter results suggested that neither MTD nor IL12ns dosing strategies were associated with drug-induced liver toxicity, as evidenced by the overall lack of statistically significant differences between experimental and saline control groups (File S5).

NanoString nCounter gene expression analysis – Spleen

Gene expression profiles of FFPE splenic specimens harvested at euthanasia (T7) were also examined using the same 42 gene panel on the NanoString nCounter. Following normalization using housekeeping genes *Alas1, Eef1g, G6pd, Gapdh, Hprt, Polr2a, Rpl19, and Sdha* (male

spleens) or *Eef1g, G6pd, Il2rg, Polr2a, Rpl19, and Sdha* (female spleens), differentially expressed genes, in comparison to the saline control, were analyzed (Figure S5). Intriguingly, there were minimal differentially expressed genes present within harvested spleens. Of note, the MTD group displayed significant (male - $p < 0.01$) or trending (female - $p = 0.0676$) increases in *Stat1* expression (Figure S5A). This *Stat1* expression was associated with significant increases ($p < 0.01$) in both *Gbp2* and *Cxcl9* in this same group (Figures S5B and S5E). While IFNG-related genes were increased with IL12ns dosing (in comparison to the saline control), these levels were not statistically significant. In males, the 10 mg IL12ns dosing strategy was associated with trending increases in both *Ly6g* and *Itgam* expression, with a trending decrease in *CD19* expression also apparent (Figures S5J–S5L). Overall, splenic gene expression analysis revealed minimal differences between experimental groups. Increases in *Ifng*-associated genes were apparent, with the greatest increases evident with the MTD strategy.

NanoString nCounter gene expression analysis – Lung

Gene expression profiles of FFPE lung specimens collected at euthanasia (T7) were also analyzed. Lungs were selected due to the previously observed cytokine-induced acute lung injury in the setting of systemic inflammatory response syndrome (SIRS) or cytokine storm.[74,75] Following normalization using housekeeping genes *Eef1g, G6pd, Hprt, Il2rg, Polr2a, Rpl19, and Sdha* (male) or *Eef1g, G6pd, Hprt, Polr2a, Rpl19, and Sdha* (female), differentially expressed genes, in comparison to the saline control, were further analyzed (Figure S6). Again, there were a minimal number of differentially expressed genes present amongst groups. Importantly, the female 10 mg IL12ns ($p = 0.0527$) and MTD ($p < 0.001$) groups displayed trending or significant increases in *Stat1* gene expression, respectively (Figure S6A). This increase was associated with significant ($p < 0.01$) or trending ($p = 0.0512$) increases in *Gbp2* and *Gbp3* expression within the female MTD group, respectively (Figures S6B and S6C). Furthermore, the female MTD group also displayed trending increases in both *Cxcl9* (Figure S6E) and *PD-L1* (Figure S6H), indicating signs of exhaustive pro-inflammatory signaling within lung tissues. Lastly, the 10 mg IL12ns group displayed a significant increase ($p < 0.05$) in *Itgam* expression, however, only within female mice. Overall, these data suggest that the IL12ns dosing strategy may not cause SIRS-associated acute lung injury in a short-duration treatment setting, as measured by the lack of pro-inflammatory signaling within this tissue. While subtle, MTD, in contrast, increased both pro-inflammatory *Ifng* signaling alongside the immune checkpoint molecule *PD-L1* within harvested lungs. These changes ultimately correlate with the previously described systemic immune findings with MTD strategy and indicate development of SIRS-like inflammatory insults as seen in the setting of acute lung injury.[76]

DISCUSSION AND CONCLUSION

The purpose of this study was to assess the immunotoxicity of IL12ns in healthy male and female BALB/c mice while examining the pharmacodynamics of nanosphere cytokine delivery. While histopathological and NanoString nCounter analysis supports that neither MTD nor IL12ns therapy drove pathological, drug-induced necrosis within examined tissues, the deployment of a rigorous IDP detailed numerous immunological differences between these dosing strategies. At the forefront of these differences was pathologic peripheral overstimulation with the MTD strategy, as evidenced by signs of immune exhaustion and inflammatory cell death. Accordingly, findings from the IDP can be grouped into three, often overlapping, categories: (1) immunologic markers associated with undesirable peripheral immune activation, (2) immunologic markers that may allow for IL12ns dose titration in a clinical setting, and (3) immunologic markers which support the necessity of the IL12ns vector delivery system and the proposed pharmacodynamic mechanism of action.

First, IDP analysis revealed numerous markers associated with peripheral immune overstimulation, as measured within the bolus MTD group. It is well understood that upon exposure to IFN-γ expression of numerous immune inhibitory molecules, such as PD-L1, are upregulated.[17] Expression of CD86, CEACAM-1, and class II MHC molecules, the ligands for immunosuppressive checkpoint inhibitors CTLA-4, TIM-3, and LAG3, respectively, are also increased in response to IFN-γ.[77] Accordingly, our study reports an increase in neutrophil PD-L1 expression alongside peripheral IFN-γ and associated chemokines with the bolus MTD strategy. PD-L1+ neutrophils have been associated with decreased cytotoxicity in the setting of cancer[32] and worsening severity of autoimmune disorders.[78] Further, the MTD strategy was also associated with increases in % PD-L1+, % CD66b+, % $CD80^+$, and % MHC-II+ PMN-MDSCs. This observation likely indicates bone marrow release of an immature, granulocytic myeloid population with heightened immunosuppressive capacity in the setting of IL-12 overstimulation.[79,80] Additionally, while IL-12 stimulus initially drives NK cell activation, high-dose administration of IL-12 was associated with the induction of NK cell apoptosis and decreasing levels of STAT4 mRNA.[50] Increases in Ki67+ NK cells with high-dose IL-12 administration, previously associated with autoimmunity and its severity,[81] may further indicate the initiation of pathological overstimulation with unencapsulated IL-12 therapy.[82]

Moreover, plasma cytokine and chemokine changes, as depicted in the MTD group, recapitulate the previous immunotoxicity evident in human clinical trials.[23] Decreases in circulating IFN-γ, and subsequent declines in both CXCL9 and CXCL10, were observed with repeated unencapsulated IL-12 stimulation in the MTD group.[23] Maintaining elevated IFN-γ levels throughout IL-12 treatment was rare, however, associated with anti-tumor responses in previous human clinical trials.[83] In support of this assertion, the activation of compensatory mechanisms and generation of an exhaustive, hyporesponsive phenotype were also observed with MTD delivery. The early increase in plasma IFN-γ was associated with increases in PBMC *Il10* gene expression. IL-10 is a critical immunomodulatory cytokine known for its immunosuppressive effects[84] and is associated with downregulation of IL-12 and other pro-inflammatory signaling pathways.[85] MTD also increased expression of lymphoid immune exhaustion genes (*CTLA-4*, *Lag3*, and *Havcr2* or *Tim-3*), suggesting the development of a hyporesponsive gene signature within peripheral immune cells.[86] The sustained expression of *Socs1*, a negative regulator of IFN-γ signaling responsible for preventing damaging pro-inflammatory immune responses,[87–91] with the MTD strategy further suggests compensatory downregulation of IFN-γ signaling in peripheral immune cells.

Secondly, immunologic markers for IL12ns dose titration were also identified. Peripheral blood assessments made 12 h post-IL12ns injection (T2, T4, and T6) were associated with two distinct cellular changes. Specifically, the 10 mg IL12ns group exhibited increases in myeloid lineage cells (particularly neutrophils) positive for iNOS (NOS2)[33] and, at early timepoints, Arg-1 (ARG).[92] Of note, elevated levels of polymorphonuclear (PMN) cells was observed to be crucial for disruption of tumor vessels in the setting of systemic IL-12 therapy.[20] Activated neutrophils, however, can inhibit T-lymphocyte functions through release of Arg-1 and subsequent depletion of the integral amino acid L-arginine.[93] These cells can also directly inhibit T cell activation by cell–cell interactions through the PD-L1/PD-1 axis, which is upregulated in response to IFN-γ stimulation.[94,95] Therefore, observing PMN-related increases in peripheral blood should still be considered a positive immune response to systemic IL-12 therapy. However, ensuring that these IL-6-induced neutrophils lack PD-L1 expression (as seen in MTD), do not attain markedly increased Arg-1 expression, and return to near-physiological levels post-injection (as evident in this study) will likely be crucial immunological markers used for IL12ns dose titration in future human clinical trials. Coincidentally, B-lymphocytes experienced an opposite trend. The associated declines in % $CD19^+$ B-lymphocytes are likely the result of B cell recruitment to peripheral sites of inflammation, acquisition of a more mature phenotype, alongside a bone marrow shift favoring myelopoiesis in the setting of an acute inflammatory response as seen in infection.[96]

As previously indicated, IL12ns dosing was also associated with elevated plasma levels of the inflammatory cytokines IL-6[97–99] and TNF-α.[100] IL-6 stimulates the production of most acute phase proteins in the acute-phase reaction.[101] Importantly, the detrimental effects of IL-6 in the setting of chronic inflammation are associated with persistent, not transient, elevation of this cytokine.[102] In this study, IL-6 plasma cytokine levels were increased 12 h post-10 mg IL12ns dosing timepoints (T2, T4, T6), however, returned to baseline thereafter (T3, T5, T7). While an elevation in IL-6 confirms successful initiation of a desired tissue-resident inflammatory response with IL12ns dosing, monitoring its levels over the course of therapy will likely be critical for the prevention of chronic inflammation and development of SIRS-like immunophenotype.[103,104] Similar consideration must also be made for the complementary pleiotropic inflammatory cytokine, TNF-α.[38,105]

Lastly, the combination of plasma protein and transcriptomic analysis further indicates support for the proposed pharmacodynamic mechanism of IL12ns. While plasma proteomic measurements encompass those cytokines and chemokines released from numerous cellular sources,[106–110] bulk RNA-seq analysis was performed on total RNA isolated from a PBMC single cell suspension. This distinction ultimately allows discernment of a plasma protein's source (cells of tissue or peripheral blood) and the likely location of signaling pathway activation. Intriguingly, while plasma protein analysis indicated drastic increases in circulating IL-6 levels with 10 mg IL12ns dosing (not evident within the MTD group), bulk PBMC RNA-seq analysis revealed limited to no differences in *Il6* expression amongst experimental groups. These findings suggest that the source of this acute phase protein is likely tissue-resident cells (hepatocytes of the liver, fibroblasts at sites of inflammation[99,102]), responding to IL12ns tissue deposition and activation, however not by activation of cells within the periphery (blood immune cells/endothelial cells). A similar relationship of increased plasma protein with minimal differences in PBMC gene expression was apparent for TNF-α and inflammatory chemokines CCL2, CCL3, and CCL4.[111–114]

Additionally, previous literature suggests that CXCL10, in direct response to IFN-γ, is secreted predominantly by immune cells (leukocytes, activated neutrophils, monocytes), followed by fibroblasts, keratinocytes, epithelial, and endothelial cells.[115–118] Peripheral blood plasma analysis revealed that while plasma levels of this chemokine are elevated within the MTD group, these levels were eventually exceeded by the 10 mg IL12ns group at later dosing timepoints. Importantly, bulk PBMC RNA-seq analysis demonstrated that while these elevated CXCL10 chemokine levels (from plasma) are associated with increased *Cxcl10* gene expression (from circulating PBMCs) in the MTD group, only plasma CXCL10 levels are increased with 10 mg IL12ns dosing. The associated *Cxcl10* gene expression increase in PBMCs was not measured with IL12ns dosing. This finding ultimately suggests that IL12ns can effectively deliver IL-12 to tissue-resident immune cells, stimulate pro-inflammatory responses as measured by circulating cytokine and chemokine levels, and limit peripheral activation of circulating immune cells and the potential development of SIRS or cytokine storm.[119–122]

Due to the relatively short half-life of IL-12 and ubiquitous expression of its receptor,[18,123–125] large loading doses of the cytokine are likely required for delivery to secondary/tertiary lymphoid organs and tumor microenvironments. Here, the bolus (unencapsulated) MTD delivery strategy recapitulated the immune findings from previous human clinical trials[23,24,126]: peripheral immune stimulation with repeated bolus IL-12 dosing induces initial pro-inflammatory responses that eventually result in the development of an exhausted, immunotoxic immune profile. Conversely, our data suggests that IL12ns prevent aberrant peripheral blood activation by shielding IL-12 from peripheral immune cells. This protective effect is likely due to the near immediate tissue deposition of the PLGA vector system[64,65] and slow, controlled cytokine elution thereafter.[30] This efficient vector delivery system presumably reduces the overall dose required for desired tissue delivery and anti-tumor efficacy.

This phenomenon was ultimately supported by our NanoString nCounter gene expression profiling of harvested liver, spleen, and lung specimens. Here, IL12ns drove tissue-resident increases in pro-inflammatory IFNG and IL-6 gene expression alongside the chemokines associated with immune cell recruitment. Importantly, this tissue-resident pro-inflammatory signaling from IL12ns was accomplished without inducing overt immune exhaustion locally nor within peripheral blood. While the MTD strategy vastly increased expression of many pro-inflammatory genes within analyzed tissues, these increases (particularly in liver and lung) were accompanied by compensatory checkpoint inhibitor expression indicative of an exhaustive immunophenotype. The increases in pro-inflammatory cytokine/chemokine signatures without co-expression of these inhibitory molecules, even days (T7) after the last IL12ns dose (T6), emphasizes the importance of slow and controlled IL-12 release after IL12ns deposition as a crucial pharmacodynamic feature of this vector system. While there were limited differentially expressed genes within lung specimens, the lack of both pro-inflammatory and immune checkpoint inhibitor expression (as seen with MTD) further supports that IL12ns can prevent SIRS or cytokine storm-associated pathologies such as cytokine-induced acute lung injury.[74] The

increase in myeloid infiltration with IL12ns dosing will require further investigation in long duration treatment studies, however, may be crucial to pro-tumoral vessel destruction in the prevention of metastatic disease, as previously observed.[20] Ultimately, this multi-organ gene expression analysis further supports that IL12ns can drive healthy and sustained pro-inflammatory signaling systemically within tissues while preventing overt immunologic toxicity in peripheral blood.

In conclusion, the combined proteomic, transcriptomic, and histopathological analyses ultimately support the proposed mechanistic efficacy of the IL12ns vector delivery system. To our knowledge, these data are the first to exemplify the effects of differential pharmacodynamics (nanosphere, encapsulated versus bolus, unencapsulated) on systemic immune responses during cytokine-based immunotherapy. Importantly, these immunological responses, seen in the IL12ns cohorts, correlate with the efficacious, anti-tumor immune adaptations known to be important in systemic IL-12 therapy including (1) the ability to drive effector signaling within systemic immune organs, as measured by increases in proinflammatory cytokines (IFN-γ, IL-6), (2) production of anti-angiogenic chemokines (CXCL9, CXCL10), and (3) activation of polymorphonuclear cells (neutrophils) for destruction of tumor blood vessels.[20] These responses occur all while avoiding the clinical toxicity seen with the MTD strategy. Deployment of this IDP and reaffirmation of these findings in *in vivo* models of various solid tumors is ultimately warranted and will be the basis of future investigations.

Limitations of the study

While robust in its analyses, our study has inherent limitations. Of note, this study only investigated the delivery of a single pro-inflammatory cytokine (IL-12). Whether the immune protective effects of vector encapsulation will translate to other antibody- and cytokine-based therapies has yet to be examined. Furthermore, the IL12ns dosing strategy was delivered at a previously determined maximally concentrated dose of 40 mg/mL (10 mg in 250 μL). The 10 mg IL12ns dose delivers approximately 20% of the MTD (~1600 ng/kg/day IL-12 versus 10,000 ng/kg/day IL-12), to which many of these immunological comparisons were made. Future studies directly comparing the resulting immunological changes between IL12ns and matched bolus doses are warranted. Additionally, while both male and female immune responses are examined in this study, statistical analysis was limited to intersex comparisons between experimental groups. The choice to stratify the sexes during analysis was multifold including simplicity of conveying experimental results, opportunity to determine sex-specific biomarkers, with existing literature suggesting known sex differences in immune responses,[127] and ultimately providing rigor to our findings, with similar observations evident in both sexes. Direct comparisons between male and female immune responses, however, may be warranted before further investigation. Finally, these analyses were performed in only one model (healthy male and female BALB/c mice), which may limit the generalizability of our findings. Additional investigation using other models (murine, canine, non-human primates) may ultimately be warranted.

STAR★METHODS

Detailed methods are provided in the online version of this paper and include the following:

- KEY RESOURCES TABLE
- RESOURCE AVAILABILITY
  - Lead contact
  - Materials availability
  - Data and code availability
- EXPERIMENTAL MODEL AND STUDY PARTICIPANT DETAILS
- METHOD DETAILS
  - Experimental design
  - IL12ns and rmIL-12 administration
  - Peripheral blood collection
  - Synthesis of IL12ns
  - IL12ns characterization
  - Clinical moribundity and mortality observations
  - Spectral flow cytometric analysis
  - Plasma analysis via BioLegend LegendPlex
  - RNA extraction, library preparation, and next-generation sequencing of PBMCs
  - Bulk PBMC RNA-seq analysis
  - Necropsy and histopathology assessment
  - RNA extraction from formalin-fixed, paraffin embedded liver, spleen, and lung specimens
  - NanoString nCounter analysis of formalin-fixed, paraffin-embedded liver, spleen, and lung specimens
- QUANTIFICATION AND STATISTICAL ANALYSIS

SUPPLEMENTAL INFORMATION

Supplemental information can be found online at https://doi.org/10.1016/j.isci.2024.108836.

ACKNOWLEDGMENTS

We acknowledge the use of the WVU Shared Research Facilities, University of Virginia Flow Cytometry Core (RRID: SCR_017829), University of Virginia Genome Analysis and Technology Core (RRID:SCR_018883), and University of Virginia School of Medicine Spatial Biology Core Facility (RRID:SCR_023281). This work was supported by Pittsburgh Cure Sarcoma, ICaPath Inc., the WVU Flow Cytometry & Single Cell Core Facility through NIH CoBRE (grant P20GM121322 and P20GM109098) and WVCTSI [P20GM103434 - West Virginia IDeA Network of Biomedical Research Excellence (WV-INBRE)], as well as the WVU Bioinformatics Core through NIH NIGMS (P20 GM103434 and U54 GM-104942).

AUTHOR CONTRIBUTIONS

Conceptualization, R.A.L. and B.A.L.; Methodology, R.A.L., M.G.H., and B.A.L.; Software, S.A.D., H.A., and M.G.H.; Formal Analysis, R.A.L., S.A.D., E.C., J.J.P., C.C., G.H., E.K., M.A.N., A.O., S.P.S., and B.A.L.; Investigation, R.A.L., S.A.D., A.S., E.C., J.V.H., J.B.H., A.P., Y.B., K.S., A.O., and B.A.L.; Resources, R.A.L., A.S., and B.A.L.; Data Curation, R.A.L., S.A.D., H.A., and M.G.H.; Writing – Original Draft, R.A.L., S.A.D., C.C., A.S., K.S., G.H., and M.A.N.; Writing – Review and Editing, R.A.L., S.A.D., E.C., J.J.P., J.B.H., J.V.H., C.C., E.K., A.O., M.G.H., S.P.S., and B.A.L.; Visualization, R.A.L. and S.A.D.; Supervision, R.A.L., A.S., and B.A.L.; Project Administration, R.A.L., A.S., and B.A.L.; Funding Acquisition, B.A.L.

DECLARATION OF INTERESTS

B.A.L., is founder and Chief Scientific Officer of ICaPath Inc., which holds the worldwide exclusive license to the technology presented from West Virginia University Research Corporation (Patent: PROTEIN-LOADED PLGA NANOSPHERES. PCT/US2020/063314. WO2021/113638A1). All other authors declare no competing interests.

Received: September 26, 2023
Revised: November 4, 2023
Accepted: January 3, 2024
Published: January 9, 2024

REFERENCES

1. Ribatti, D. (2017). The concept of immune surveillance against tumors. The first theories. Oncotarget *8*, 7175–7180.
2. Dunn, G.P., Bruce, A.T., Ikeda, H., Old, L.J., and Schreiber, R.D. (2002). Cancer immunoediting: from immunosurveillance to tumor escape. Nat. Immunol. *3*, 991–998.
3. Dunn, G.P., Old, L.J., and Schreiber, R.D. (2004). The immunobiology of cancer immunosurveillance and immunoediting. Immunity *21*, 137–148.
4. Dunn, G.P., Old, L.J., and Schreiber, R.D. (2004). The three Es of cancer immunoediting. Annu. Rev. Immunol. *22*, 329–360.
5. Beatty, G.L., and Gladney, W.L. (2015). Immune escape mechanisms as a guide for cancer immunotherapy. Clin. Cancer Res. *21*, 687–692.
6. Markel, J.E., Noore, J., Emery, E.J., Bobnar, H.J., Kleinerman, E.S., and Lindsey, B.A. (2018). Using the spleen as an in vivo systemic immune barometer alongside osteosarcoma disease progression and immunotherapy with α-PD-L1. Sarcoma *2018*, 8694397.
7. Lafleur, E.A., Jia, S.F., Worth, L.L., Zhou, Z., Owen-Schaub, L.B., and Kleinerman, E.S. (2001). Interleukin (IL)-12 and IL-12 gene transfer up-regulate Fas expression in human osteosarcoma and breast cancer cells. Cancer Res. *61*, 4066–4071.
8. Brunda, M.J., Luistro, L., Warrier, R.R., Wright, R.B., Hubbard, B.R., Murphy, M., Wolf, S.F., and Gately, M.K. (1993). Antitumor and antimetastatic activity of interleukin 12 against murine tumors. J. Exp. Med. *178*, 1223–1230.
9. Brunda, M.J., Luistro, L., Rumennik, L., Wright, R.B., Dvorozniak, M., Aglione, A., Wigginton, J.M., Wiltrout, R.H., Hendrzak, J.A., and Palleroni, A.V. (1996). Antitumor activity of interleukin 12 in preclinical models. Cancer Chemother. Pharmacol. *38*, S16–S21.
10. Worth, L.L., Lafleur, E.A., Jia, S.F., and Kleinerman, E.S. (2002). Fas expression inversely correlates with metastatic potential in osteosarcoma cells. Oncol. Rep. *9*, 823–827.
11. Jia, S.F., Worth, L.L., Densmore, C.L., Xu, B., Duan, X., and Kleinerman, E.S. (2003). Aerosol gene therapy with PEI: IL-12 eradicates osteosarcoma lung metastases. Clin. Cancer Res. *9*, 3462–3468.
12. Saha, D., Martuza, R.L., and Rabkin, S.D. (2017). Macrophage Polarization Contributes to Glioblastoma Eradication by Combination Immunovirotherapy and Immune Checkpoint Blockade. Cancer Cell *32*, 253–267.e5.
13. Saha, D., Wakimoto, H., Peters, C.W., Antoszczyk, S.J., Rabkin, S.D., and Martuza, R.L. (2018). Combinatorial Effects of VEGFR Kinase Inhibitor Axitinib and Oncolytic Virotherapy in Mouse and Human Glioblastoma Stem-Like Cell Models. Clin. Cancer Res. *24*, 3409–3422.
14. Saha, D., Martuza, R.L., and Rabkin, S.D. (2018). Oncolytic herpes simplex virus immunovirotherapy in combination with immune checkpoint blockade to treat glioblastoma. Immunotherapy *10*, 779–786.
15. Zhang, W., Fulci, G., Wakimoto, H., Cheema, T.A., Buhrman, J.S., Jeyaretna, D.S., Stemmer Rachamimov, A.O., Rabkin, S.D., and Martuza, R.L. (2013). Combination of oncolytic herpes simplex viruses armed with angiostatin and IL-12 enhances antitumor efficacy in human glioblastoma models. Neoplasia *15*, 591–599.
16. Mortezaee, K., and Majidpoor, J. (2022). Roles for macrophage-polarizing interleukins in cancer immunity and immunotherapy. Cell. Oncol. *45*, 333–353.
17. Morinobu, A., Gadina, M., Strober, W., Visconti, R., Fornace, A., Montagna, C., Feldman, G.M., Nishikomori, R., and O'Shea, J.J. (2002). STAT4 serine phosphorylation is critical for IL-12-induced IFN-gamma production but not for cell proliferation. Proc. Natl. Acad. Sci. USA *99*, 12281–12286.
18. Watford, W.T., Moriguchi, M., Morinobu, A., and O'Shea, J.J. (2003). The biology of IL-12: coordinating innate and adaptive immune responses. Cytokine Growth Factor Rev. *14*, 361–368.
19. Albini, A., Brigati, C., Ventura, A., Lorusso, G., Pinter, M., Morini, M., Mancino, A., Sica, A., and Noonan, D.M. (2009). Angiostatin anti-angiogenesis requires IL-12: the innate immune system as a key target. J. Transl. Med. *7*, 5.
20. Cavallo, F., Di Carlo, E., Butera, M., Verrua, R., Colombo, M.P., Musiani, P., and Forni, G. (1999). Immune events associated with the cure of established tumors and spontaneous metastases by local and systemic interleukin 12. Cancer Res. *59*, 414–421.
21. Atkins, M.B., Robertson, M.J., Gordon, M., Lotze, M.T., DeCoste, M., DuBois, J.S., Ritz, J., Sandler, A.B., Edington, H.D., Garzone, P.D., et al. (1997). Phase I evaluation of intravenous recombinant human interleukin

12 in patients with advanced malignancies. Clin. Cancer Res. *3*, 409–417.
22. Nguyen, K.G., Vrabel, M.R., Mantooth, S.M., Hopkins, J.J., Wagner, E.S., Gabaldon, T.A., and Zaharoff, D.A. (2020). Localized Interleukin-12 for Cancer Immunotherapy. Front. Immunol. *11*, 575597.
23. Portielje, J.E.A., Lamers, C.H.J., Kruit, W.H.J., Sparreboom, A., Bolhuis, R.L.H., Stoter, G., Huber, C., and Gratama, J.W. (2003). Repeated administrations of interleukin (IL)-12 are associated with persistently elevated plasma levels of IL-10 and declining IFN-gamma, tumor necrosis factor-alpha, IL-6, and IL-8 responses. Clin. Cancer Res. *9*, 76–83.
24. Cohen, J. (1995). IL-12 deaths: explanation and a puzzle. Science *270*, 908.
25. Robertson, M.J., Cameron, C., Atkins, M.B., Gordon, M.S., Lotze, M.T., Sherman, M.L., and Ritz, J. (1999). Immunological effects of interleukin 12 administered by bolus intravenous injection to patients with cancer. Clin. Cancer Res. *5*, 9–16.
26. Pratt, H.G., Justin, E.M., and Lindsey, B.A. (2020). Applying Osteosarcoma Immunology to Understand Disease Progression and Assess Immunotherapeutic Response. Adv. Exp. Med. Biol. *1258*, 91–109.
27. Gollob, J.A., Mier, J.W., Veenstra, K., McDermott, D.F., Clancy, D., Clancy, M., and Atkins, M.B. (2000). Phase I trial of twice-weekly intravenous interleukin 12 in patients with metastatic renal cell cancer or malignant melanoma: ability to maintain IFN-gamma induction is associated with clinical response. Clin. Cancer Res. *6*, 1678–1692.
28. Garrett-Mayer, E., and June 24. (2022). Dose Optimization for Anti-cancer Agents in the Era of Immunotherapy and Targeted Agents (held in Alexandria, VA: American Society of Clinical Oncology)).
29. Markel, J.E., Lacinski, R.A., and Lindsey, B.A. (2020). Nanocapsule Delivery of IL-12. Adv. Exp. Med. Biol. *1257*, 155–168.
30. Lacinski, R.A., Markel, J.E., Pratt, H.G., Reinbeau, R.M., Stewart, A., Santiago, S.P., and Lindsey, B.A. (2023). Optimizing the Synthesis of Interleukin-12-loaded PLGA Nanospheres (rmIL-12ns) via Ultrasonication for Treatment of Metastatic Osteosarcoma. J. Orthop. Res. *41*, 1565–1581.
31. Lacinski, R.A., Markel, J.E., Noore, J., Pratt, H.G., and Lindsey, B.A. (2022). Synthesis, Characterization, and. J. Immunol. Res. *2022*, 6993187.
32. Yajuk, O., Baron, M., Toker, S., Zelter, T., Fainsod-Levi, T., and Granot, Z. (2021). The PD-L1/PD-1 Axis Blocks Neutrophil Cytotoxicity in Cancer. Cells *10*.
33. Saini, R., and Singh, S. (2019). Inducible nitric oxide synthase: An asset to neutrophils. J. Leukoc. Biol. *105*, 49–61.
34. Solito, S., Bronte, V., and Mandruzzato, S. (2011). Antigen specificity of immune suppression by myeloid-derived suppressor cells. J. Leukoc. Biol. *90*, 31–36.
35. Yang, Y., Li, C., Liu, T., Dai, X., and Bazhin, A.V. (2020). Myeloid-Derived Suppressor Cells in Tumors: From Mechanisms to Antigen Specificity and Microenvironmental Regulation. Front. Immunol. *11*, 1371.
36. Liu, C., Chu, D., Kalantar-Zadeh, K., George, J., Young, H.A., and Liu, G. (2021). Cytokines: From Clinical Significance to Quantification. Adv. Sci. *8*, e2004433.
37. Zhang, X., Edwards, J.P., and Mosser, D.M. (2006). Dynamic and transient remodeling of the macrophage IL-10 promoter during transcription. J. Immunol. *177*, 1282–1288.
38. Ma, X. (2001). TNF-alpha and IL-12: a balancing act in macrophage functioning. Microb. Infect. *3*, 121–129.
39. Gillespie, M., Jassal, B., Stephan, R., Milacic, M., Rothfels, K., Senff-Ribeiro, A., Griss, J., Sevilla, C., Matthews, L., Gong, C., et al. (2022). The reactome pathway knowledgebase 2022. Nucleic Acids Res. *50*, D687–D692.
40. Garapati, P.V. (2010). Interferon gamma signaling (Reactome), p. 83.
41. Jupe, S., and Duenas, C. (2017). Interleukin-12 signaling (Reactome), p. 83.
42. Jupe, S. (2016). 57, Interleukin-10 signaling (Reactome).
43. Shamovsky, V. TNF signaling. Reactome. .
44. Liberzon, A., Birger, C., Thorvaldsdóttir, H., Ghandi, M., Mesirov, J.P., and Tamayo, P. (2015). The Molecular Signatures Database (MSigDB) hallmark gene set collection. Cell Syst. *1*, 417–425.
45. Bergsbaken, T., Fink, S.L., and Cookson, B.T. (2009). Pyroptosis: host cell death and inflammation. Nat. Rev. Microbiol. *7*, 99–109.
46. Liu, Z., Wang, C., and Lin, C. (2023). Pyroptosis as a double-edged sword: The pathogenic and therapeutic roles in inflammatory diseases and cancers. Life Sci. *318*, 121498.
47. Rao, Z., Zhu, Y., Yang, P., Chen, Z., Xia, Y., Qiao, C., Liu, W., Deng, H., Li, J., Ning, P., and Wang, Z. (2022). Pyroptosis in inflammatory diseases and cancer. Theranostics *12*, 4310–4329.
48. Wei, X., Xie, F., Zhou, X., Wu, Y., Yan, H., Liu, T., Huang, J., Wang, F., Zhou, F., and Zhang, L. (2022). Role of pyroptosis in inflammation and cancer. Cell. Mol. Immunol. *19*, 971–992.
49. Ramana, C.V., Gil, M.P., Schreiber, R.D., and Stark, G.R. (2002). Stat1-dependent and -independent pathways in IFN-gamma-dependent signaling. Trends Immunol. *23*, 96–101.
50. Huang, Y., Lei, Y., Zhang, H., Zhang, M., and Dayton, A. (2011). Interleukin-12 treatment down-regulates STAT4 and induces apoptosis with increasing ROS production in human natural killer cells. J. Leukoc. Biol. *90*, 87–97.
51. Robinson, R.T. (2015). IL12Rβ1: the cytokine receptor that we used to know. Cytokine *71*, 348–359.
52. Pardoux, C., Ma, X., Gobert, S., Pellegrini, S., Mayeux, P., Gay, F., Trinchieri, G., and Chouaib, S. (1999). Downregulation of interleukin-12 (IL-12) responsiveness in human T cells by transforming growth factor-beta: relationship with IL-12 signaling. Blood *93*, 1448–1455.
53. Dinarello, C.A., Novick, D., Kim, S., and Kaplanski, G. (2013). Interleukin-18 and IL-18 binding protein. Front. Immunol. *4*, 289.
54. Bui, T.M., Wiesolek, H.L., and Sumagin, R. (2020). ICAM-1: A master regulator of cellular responses in inflammation, injury resolution, and tumorigenesis. J. Leukoc. Biol. *108*, 787–799.
55. Figenschau, S.L., Knutsen, E., Urbarova, I., Fenton, C., Elston, B., Perander, M., Mortensen, E.S., and Fenton, K.A. (2018). ICAM1 expression is induced by proinflammatory cytokines and associated with TLS formation in aggressive breast cancer subtypes. Sci. Rep. *8*, 11720.
56. Zella, D., Barabitskaja, O., Burns, J.M., Romerio, F., Dunn, D.E., Revello, M.G., Gerna, G., Reitz, M.S., Gallo, R.C., and Weichold, F.F. (1998). Interferon-gamma increases expression of chemokine receptors CCR1, CCR3, and CCR5, but not CXCR4 in monocytoid U937 cells. Blood *91*, 4444–4450.
57. Hutchins, A.P., Diez, D., and Miranda-Saavedra, D. (2013). The IL-10/STAT3-mediated anti-inflammatory response: recent developments and future challenges. Brief. Funct. Genomics *12*, 489–498.
58. Braun, D.A., Fribourg, M., and Sealfon, S.C. (2013). Cytokine response is determined by duration of receptor and signal transducers and activators of transcription 3 (STAT3) activation. J. Biol. Chem. *288*, 2986–2993.
59. Qin, C.C., Liu, Y.N., Hu, Y., Yang, Y., and Chen, Z. (2017). Macrophage inflammatory protein-2 as mediator of inflammation in acute liver injury. World J. Gastroenterol. *23*, 3043–3052.
60. Harris, S.G., Padilla, J., Koumas, L., Ray, D., and Phipps, R.P. (2002). Prostaglandins as modulators of immunity. Trends Immunol. *23*, 144–150.
61. Kalinski, P. (2012). Regulation of immune responses by prostaglandin E2. J. Immunol. *188*, 21–28.
62. Sajiki, Y., Konnai, S., Okagawa, T., Nishimori, A., Maekawa, N., Goto, S., Watari, K., Minato, E., Kobayashi, A., Kohara, J., et al. (2019). Prostaglandin E_2-Induced Immune Exhaustion and Enhancement of Antiviral Effects by Anti-PD-L1 Antibody Combined with COX-2 Inhibitor in Bovine Leukemia Virus Infection. J. Immunol. *203*, 1313–1324.
63. Sajiki, Y., Konnai, S., Watari, K., Okagawa, T., Tanaka, A., Kawaji, S., Nagata, R., Maekawa, N., Suzuki, Y., Kato, Y., et al. (2022). Prostaglandin E_2-Induced Immune Suppression via Cytotoxic T-Lymphocyte Antigen 4 in Paratuberculosis. Infect. Immun. *90*, e0021022.
64. Semete, B., Booysen, L., Lemmer, Y., Kalombo, L., Katata, L., Verschoor, J., and Swai, H.S. (2010). In vivo evaluation of the biodistribution and safety of PLGA nanoparticles as drug delivery systems. Nanomedicine. *6*, 662–671.
65. Fonseca-Gomes, J., Loureiro, J.A., Tanqueiro, S.R., Mouro, F.M., Ruivo, P., Carvalho, T., Sebastião, A.M., Diógenes, M.J., and Pereira, M.C. (2020). In vivo Bio-Distribution and Toxicity Evaluation of Polymeric and Lipid-Based Nanoparticles: A Potential Approach for Chronic Diseases Treatment. Int. J. Nanomed. *15*, 8609–8621.
66. Alexis, F., Pridgen, E., Molnar, L.K., and Farokhzad, O.C. (2008). Factors affecting the clearance and biodistribution of polymeric nanoparticles. Mol. Pharm. *5*, 505–515.
67. Alonaizan, R., Woods, S., Hargrave, K.E., and Roberts, C.W. (2021). An Exaggerated Immune Response in Female BALB/c Mice Controls Initial. Pathogens *10*.
68. Schmidt-Arras, D., and Rose-John, S. (2016). IL-6 pathway in the liver: From physiopathology to therapy. J. Hepatol. *64*, 1403–1415.
69. Carr, M.W., Roth, S.J., Luther, E., Rose, S.S., and Springer, T.A. (1994). Monocyte chemoattractant protein 1 acts as a T-lymphocyte chemoattractant. Proc. Natl. Acad. Sci. USA *91*, 3652–3656.

70. Andrews, L.P., Yano, H., and Vignali, D.A.A. (2019). Inhibitory receptors and ligands beyond PD-1, PD-L1 and CTLA-4: breakthroughs or backups. Nat. Immunol. *20*, 1425–1434.
71. Carow, B., and Rottenberg, M.E. (2014). SOCS3, a Major Regulator of Infection and Inflammation. Front. Immunol. *5*, 58.
72. Duncan, S.A., Sahu, R., Dixit, S., Singh, S.R., and Dennis, V.A. (2020). Suppressors of Cytokine Signaling (SOCS)1 and SOCS3 Proteins Are Mediators of Interleukin-10 Modulation of Inflammatory Responses Induced by. Mediat. Inflamm. *2020*, 7461742.
73. Davis, A.P., Wiegers, T.C., Johnson, R.J., Sciaky, D., Wiegers, J., and Mattingly, C.J. (2023). Comparative Toxicogenomics Database (CTD): update 2023. Nucleic Acids Res. *51*, D1257–D1262.
74. Goodman, R.B., Pugin, J., Lee, J.S., and Matthay, M.A. (2003). Cytokine-mediated inflammation in acute lung injury. Cytokine Growth Factor Rev. *14*, 523–535.
75. Hukkanen, R.R., Liggitt, H.D., Murnane, R.D., and Frevert, C.W. (2009). Systemic inflammatory response syndrome in nonhuman primates culminating in multiple organ failure, acute lung injury, and disseminated intravascular coagulation. Toxicol. Pathol. *37*, 799–804.
76. Lomas-Neira, J., Monaghan, S.F., Huang, X., Fallon, E.A., Chung, C.S., and Ayala, A. (2018). Novel Role for PD-1:PD-L1 as Mediator of Pulmonary Vascular Endothelial Cell Functions in Pathogenesis of Indirect ARDS in Mice. Front. Immunol. *9*, 3030.
77. Kursunel, M.A., and Esendagli, G. (2016). The untold story of IFN-γ in cancer biology. Cytokine Growth Factor Rev. *31*, 73–81.
78. Luo, Q., Huang, Z., Ye, J., Deng, Y., Fang, L., Li, X., Guo, Y., Jiang, H., Ju, B., Huang, Q., and Li, J. (2016). PD-L1-expressing neutrophils as a novel indicator to assess disease activity and severity of systemic lupus erythematosus. Arthritis Res. Ther. *18*, 47.
79. Brandau, S., Trellakis, S., Bruderek, K., Schmaltz, D., Steller, G., Elian, M., Suttmann, H., Schenck, M., Welling, J., Zabel, P., and Lang, S. (2011). Myeloid-derived suppressor cells in the peripheral blood of cancer patients contain a subset of immature neutrophils with impaired migratory properties. J. Leukoc. Biol. *89*, 311–317.
80. Veglia, F., Sanseviero, E., and Gabrilovich, D.I. (2021). Myeloid-derived suppressor cells in the era of increasing myeloid cell diversity. Nat. Rev. Immunol. *21*, 485–498.
81. Hudspeth, K., Wang, S., Wang, J., Rahman, S., Smith, M.A., Casey, K.A., Autoimmunity Molecular Team, Manna, Z., Sanjuan, M., Kolbeck, R., et al. (2019). Natural killer cell expression of Ki67 is associated with elevated serum IL-15, disease activity and nephritis in systemic lupus erythematosus. Clin. Exp. Immunol. *196*, 226–236.
82. Barton, K.N., Siddiqui, F., Pompa, R., Freytag, S.O., Khan, G., Dobrosotskaya, I., Ajlouni, M., Zhang, Y., Cheng, J., Movsas, B., and Kwon, D. (2021). Phase I trial of oncolytic adenovirus-mediated cytotoxic and interleukin-12 gene therapy for the treatment of metastatic pancreatic cancer. Mol. Ther. Oncolytics *20*, 94–104.
83. Motzer, R.J., Rakhit, A., Thompson, J.A., Nemunaitis, J., Murphy, B.A., Ellerhorst, J., Schwartz, L.H., Berg, W.J., and Bukowski, R.M. (2001). Randomized multicenter phase II trial of subcutaneous recombinant human interleukin-12 versus interferon-alpha 2a for patients with advanced renal cell carcinoma. J. Interferon Cytokine Res. *21*, 257–263.
84. Sabat, R. (2010). IL-10 family of cytokines. Cytokine Growth Factor Rev. *21*, 315–324.
85. Ma, X., Yan, W., Zheng, H., Du, Q., Zhang, L., Ban, Y., Li, N., and Wei, F. (2015). Regulation of IL-10 and IL-12 Production and Function in Macrophages and Dendritic Cells. F1000Res *4*.
86. Pereira, R.M., Hogan, P.G., Rao, A., and Martinez, G.J. (2017). Transcriptional and epigenetic regulation of T cell hyporesponsiveness. J. Leukoc. Biol. *102*, 601–615.
87. Alexander, W.S., Starr, R., Fenner, J.E., Scott, C.L., Handman, E., Sprigg, N.S., Corbin, J.E., Cornish, A.L., Darwiche, R., Owczarek, C.M., et al. (1999). SOCS1 is a critical inhibitor of interferon gamma signaling and prevents the potentially fatal neonatal actions of this cytokine. Cell *98*, 597–608.
88. Chong, M.M.W., Metcalf, D., Jamieson, E., Alexander, W.S., and Kay, T.W.H. (2005). Suppressor of cytokine signaling-1 in T cells and macrophages is critical for preventing lethal inflammation. Blood *106*, 1668–1675.
89. Fenner, J.E., Starr, R., Cornish, A.L., Zhang, J.G., Metcalf, D., Schreiber, R.D., Sheehan, K., Hilton, D.J., Alexander, W.S., and Hertzog, P.J. (2006). Suppressor of cytokine signaling 1 regulates the immune response to infection by a unique inhibition of type I interferon activity. Nat. Immunol. *7*, 33–39.
90. Alexander, W.S., Starr, R., Metcalf, D., Nicholson, S.E., Farley, A., Elefanty, A.G., Brysha, M., Kile, B.T., Richardson, R., Baca, M., et al. (1999). Suppressors of cytokine signaling (SOCS): negative regulators of signal transduction. J. Leukoc. Biol. *66*, 588–592.
91. Cornish, A.L., Davey, G.M., Metcalf, D., Purton, J.F., Corbin, J.E., Greenhalgh, C.J., Darwiche, R., Wu, L., Nicola, N.A., Godfrey, D.I., et al. (2003). Suppressor of cytokine signaling-1 has IFN-gamma-independent actions in T cell homeostasis. J. Immunol. *170*, 878–886.
92. Rosales, C. (2020). Neutrophils at the crossroads of innate and adaptive immunity. J. Leukoc. Biol. *108*, 377–396.
93. Rotondo, R., Bertolotto, M., Barisione, G., Astigiano, S., Mandruzzato, S., Ottonello, L., Dallegri, F., Bronte, V., Ferrini, S., and Barbieri, O. (2011). Exocytosis of azurophil and arginase 1-containing granules by activated polymorphonuclear neutrophils is required to inhibit T lymphocyte proliferation. J. Leukoc. Biol. *89*, 721–727.
94. de Kleijn, S., Langereis, J.D., Leentjens, J., Kox, M., Netea, M.G., Koenderman, L., Ferwerda, G., Pickkers, P., and Hermans, P.W.M. (2013). IFN-γ-stimulated neutrophils suppress lymphocyte proliferation through expression of PD-L1. PLoS One *8*, e72249.
95. Langereis, J.D., Pickkers, P., de Kleijn, S., Gerretsen, J., de Jonge, M.I., and Kox, M. (2017). Spleen-derived IFN-γ induces generation of PD-L1. J. Leukoc. Biol. *102*, 1401–1409.
96. Cain, D., Kondo, M., Chen, H., and Kelsoe, G. (2009). Effects of acute and chronic inflammation on B-cell development and differentiation. J. Invest. Dermatol. *129*, 266–277.
97. Kishimoto, T. (2006). Interleukin-6: discovery of a pleiotropic cytokine. Arthritis Res. Ther. *8* (*Suppl 2*), S2.
98. Kishimoto, T. (2010). IL-6: from its discovery to clinical applications. Int. Immunol. *22*, 347–352.
99. Tanaka, T., Narazaki, M., Masuda, K., and Kishimoto, T. (2016). Regulation of IL-6 in Immunity and Diseases. Adv. Exp. Med. Biol. *941*, 79–88.
100. Idriss, H.T., and Naismith, J.H. (2000). TNF alpha and the TNF receptor superfamily: structure-function relationship(s). Microsc. Res. Tech. *50*, 184–195.
101. Mihara, M., Hashizume, M., Yoshida, H., Suzuki, M., and Shiina, M. (2012). IL-6/IL-6 receptor system and its role in physiological and pathological conditions. Clin. Sci. *122*, 143–159.
102. Gabay, C. (2006). Interleukin-6 and chronic inflammation. Arthritis Res. Ther. *8* (*Suppl 2*), S3.
103. Giannoudis, P.V., Harwood, P.J., Loughenbury, P., Van Griensven, M., Krettek, C., and Pape, H.C. (2008). Correlation between IL-6 levels and the systemic inflammatory response score: can an IL-6 cutoff predict a SIRS state? J. Trauma *65*, 646–652.
104. Oda, S., Hirasawa, H., Shiga, H., Nakanishi, K., Matsuda, K.i., and Nakamua, M. (2005). Sequential measurement of IL-6 blood levels in patients with systemic inflammatory response syndrome (SIRS)/sepsis. Cytokine *29*, 169–175.
105. Anderson, G.M., Nakada, M.T., and DeWitte, M. (2004). Tumor necrosis factor-alpha in the pathogenesis and treatment of cancer. Curr. Opin. Pharmacol. *4*, 314–320.
106. Avirutnan, P., Malasit, P., Seliger, B., Bhakdi, S., and Husmann, M. (1998). Dengue virus infection of human endothelial cells leads to chemokine production, complement activation, and apoptosis. J. Immunol. *161*, 6338–6346.
107. Mancardi, S., Vecile, E., Dusetti, N., Calvo, E., Stanta, G., Burrone, O.R., and Dobrina, A. (2003). Evidence of CXC, CC and C chemokine production by lymphatic endothelial cells. Immunology *108*, 523–530.
108. Middleton, J., Patterson, A.M., Gardner, L., Schmutz, C., and Ashton, B.A. (2002). Leukocyte extravasation: chemokine transport and presentation by the endothelium. Blood *100*, 3853–3860.
109. Speyer, C.L., and Ward, P.A. (2011). Role of endothelial chemokines and their receptors during inflammation. J. Invest. Surg. *24*, 18–27.
110. Westra, J., Kułdo, J.M., van Rijswijk, M.H., Molema, G., and Limburg, P.C. (2005). Chemokine production and E-selectin expression in activated endothelial cells are inhibited by p38 MAPK (mitogen activated protein kinase) inhibitor RWJ 67657. Int. Immunopharmacol. *5*, 1259–1269.
111. Castellani, M.L., Bhattacharya, K., Tagen, M., Kempuraj, D., Perrella, A., De Lutiis, M., Boucher, W., Conti, P., Theoharides, T.C., Cerulli, G., et al. (2007). Anti-chemokine therapy for inflammatory diseases. Int. J. Immunopathol. Pharmacol. *20*, 447–453.
112. Conti, I., and Rollins, B.J. (2004). CCL2 (monocyte chemoattractant protein-1) and cancer. Semin. Cancer Biol. *14*, 149–154.
113. Lim, S.Y., Yuzhalin, A.E., Gordon-Weeks, A.N., and Muschel, R.J. (2016). Targeting the CCL2-CCR2 signaling axis in cancer metastasis. Oncotarget *7*, 28697–28710.

114. Menten, P., Wuyts, A., and Van Damme, J. (2002). Macrophage inflammatory protein-1. Cytokine Growth Factor Rev. *13*, 455–481.
115. Luster, A.D., and Ravetch, J.V. (1987). Biochemical characterization of a gamma interferon-inducible cytokine (IP-10). J. Exp. Med. *166*, 1084–1097.
116. Lo, B.K.K., Yu, M., Zloty, D., Cowan, B., Shapiro, J., and McElwee, K.J. (2010). CXCR3/ligands are significantly involved in the tumorigenesis of basal cell carcinomas. Am. J. Pathol. *176*, 2435–2446.
117. Liu, M., Guo, S., Hibbert, J.M., Jain, V., Singh, N., Wilson, N.O., and Stiles, J.K. (2011). CXCL10/IP-10 in infectious diseases pathogenesis and potential therapeutic implications. Cytokine Growth Factor Rev. *22*, 121–130.
118. Liu, M., Guo, S., and Stiles, J.K. (2011). The emerging role of CXCL10 in cancer (Review). Oncol. Lett. *2*, 583–589.
119. Fajgenbaum, D.C., and June, C.H. (2021). Cytokine Storm. Reply. N. Engl. J. Med. *384*, e59.
120. Dahiya, P. (2009). Burns as a model of SIRS. Front. Biosci. *14*, 4962–4967.
121. Dinarello, C.A., Gelfand, J.A., and Wolff, S.M. (1993). Anticytokine strategies in the treatment of the systemic inflammatory response syndrome. JAMA *269*, 1829–1835.
122. Shibata, M., Gonda, K., Shimura, T., Sakurai, K., and Takenoshita, S. (2018). SIRS, CARS and MARS in relationship to cancer cachexia and its clinical implications. Ann. Cancer Res. Ther. *26*, 54–59.
123. Desai, B.B., Quinn, P.M., Wolitzky, A.G., Mongini, P.K., Chizzonite, R., and Gately, M.K. (1992). IL-12 receptor. II. Distribution and regulation of receptor expression. J. Immunol. *148*, 3125–3132.
124. Lasek, W., Zagożdżon, R., and Jakobisiak, M. (2014). Interleukin 12: still a promising candidate for tumor immunotherapy? Cancer Immunol. Immunother. *63*, 419–435.
125. Scott, P. (1993). IL-12: initiation cytokine for cell-mediated immunity. Science *260*, 496–497.
126. Sacco, S., Heremans, H., Echtenacher, B., Buurman, W.A., Amraoui, Z., Goldman, M., and Ghezzi, P. (1997). Protective effect of a single interleukin-12 (IL-12) predose against the toxicity of subsequent chronic IL-12 in mice: role of cytokines and glucocorticoids. Blood *90*, 4473–4479.
127. Klein, S.L., and Flanagan, K.L. (2016). Sex differences in immune responses. Nat. Rev. Immunol. *16*, 626–638.
128. Liao, Y., Smyth, G.K., and Shi, W. (2013). The Subread aligner: fast, accurate and scalable read mapping by seed-and-vote. Nucleic Acids Res. *41*, e108.
129. Liao, Y., Smyth, G.K., and Shi, W. (2014). featureCounts: an efficient general purpose program for assigning sequence reads to genomic features. Bioinformatics *30*, 923–930.
130. Mortazavi, A., Williams, B.A., McCue, K., Schaeffer, L., and Wold, B. (2008). Mapping and quantifying mammalian transcriptomes by RNA-Seq. Nat. Methods *5*, 621–628.
131. Robinson, M.D., McCarthy, D.J., and Smyth, G.K. (2010). edgeR: a Bioconductor package for differential expression analysis of digital gene expression data. Bioinformatics *26*, 139–140.
132. Azizi, M., Farahmandghavi, F., Joghataei, M., Zandi, M., Imani, M., Bakhtiary, M., Dorkoosh, F.A., and Ghazizadeh, F. (2013). Fabrication of protein-loaded PLGA nanoparticles: effect of selected formulation variables on particle size and release profile. J. Polym. Res. *20*, 110–114.
133. Golub, J.S., Kim, Y.T., Duvall, C.L., Bellamkonda, R.V., Gupta, D., Lin, A.S., Weiss, D., Robert Taylor, W., and Guldberg, R.E. (2010). Sustained VEGF delivery via PLGA nanoparticles promotes vascular growth. Am. J. Physiol. Heart Circ. Physiol. *298*, H1959–H1965.
134. Steiner, D.F., Chen, P.H.C., and Mermel, C.H. (2021). Closing the translation gap: AI applications in digital pathology. Biochim. Biophys. Acta Rev. Canc *1875*, 188452.
135. Kulkarni, M.M. (2011). Digital multiplexed gene expression analysis using the NanoString nCounter system. Curr Protoc Mol Biol *Chapter*. Curr. Protoc. Mol. Biol. *1*. Chapter 25, Unit25B.10.
136. Geiss, G.K., Bumgarner, R.E., Birditt, B., Dahl, T., Dowidar, N., Dunaway, D.L., Fell, H.P., Ferree, S., George, R.D., Grogan, T., et al. (2008). Direct multiplexed measurement of gene expression with color-coded probe pairs. Nat. Biotechnol. *26*, 317–325.
137. Klein, S.L., and Morgan, R. (2020). The impact of sex and gender on immunotherapy outcomes. Biol. Sex Differ. *11*, 24.

STAR★METHODS

KEY RESOURCES TABLE

REAGENT or RESOURCE	SOURCE	IDENTIFIER
Antibodies		
BUV395 Mouse Anti-Ki-67, Clone B56	BD Biosciences	564071; RRID: AB_2738577
BUV563 Hamster Anti-Mouse CD69, Clone H1.2F3	BD Biosciences	741234; RRID: AB_2870786
BUV737 Rat Anti-Mouse I-A/I-E, Clone M5/114.15.2 (also known as M5/114)	BD Biosciences	748845; RRID: AB_2873248
BV480 Rat Anti-Mouse CD25, Clone PC61	BD Biosciences	566120; RRID: AB_2739522
BB515 Rat Anti-Mouse CD223, Clone C9B7W	BD Biosciences	564672; RRID: AB_2738884
BB700 Hamster Anti-Mouse CD279 (PD-1), Clone J43	BD Biosciences	566514; RRID: AB_2869777
APC-R700 Hamster Anti-Mouse CD152, Clone UC10-4F10-11	BD Biosciences	565778; RRID: AB_2739350
BB700 Rat Anti-Mouse CD86, Clone GL1	BD Biosciences	742120; RRID: AB_2871388
BUV737 Rat Anti-Mouse CD19, Clone 1D3	BD Biosciences	612781; RRID: AB_2870110
BV605 Rat Anti-Mouse CD119, Clone GR20	BD Biosciences	745111; RRID: AB_2742716
Brilliant Violet 421™ anti-mouse CD366 (Tim-3) Antibody, Clone RMT3-23	BioLegend	119723; RRID: AB_2616908
Brilliant Violet 750™ anti-mouse CD4 Antibody, Clone GK1.5	BioLegend	100467; RRID: AB_2734150
Spark Blue™ 550 anti-mouse CD8a Antibody, Clone 53–6.7	BioLegend	100780; RRID: AB_2819773
PerCP anti-mouse CD19 Antibody, Cline 6D5	BioLegend	115532; RRID: AB_2072926
PE/Dazzle™ 594 anti-mouse CD183 (CXCR3) Antibody, Clone S18001A	BioLegend	155914
PE/Cyanine7 anti-mouse CD226 (DNAM-1) Antibody, Clone 10E5	BioLegend	128812; RRID: AB_2566629
Zombie NIR™ Fixable Viability Kit	BioLegend	423105
Brilliant Violet 785™ anti-mouse CD274 (B7-H1, PD-L1) Antibody, Clone 10F.9G2	BioLegend	124331; RRID: AB_2629659
Brilliant Violet 711™ anti-mouse Ly-6G Antibody, Clone 1A8	BioLegend	127643; RRID: AB_2565971
Alexa Fluor® 700 anti-mouse I-A/I-E Antibody, Clone Clone M5/114.15.2	BioLegend	107622; RRID: AB_493727
Brilliant Violet 570™ anti-mouse Ly-6C Antibody, Clone HK1.4	BioLegend	128029; RRID: AB_10896061
PerCP anti-mouse CD11c Antibody, Clone N418	BioLegend	117326; RRID: AB_2129643
CF594 CEACAM8 antibody, polyclonal	Biorbyt	orb213728-CF594
CD80 Antibody, anti-mouse, PE-Vio® 770, REAfinity™, Clone REA983	Miltenyi Biotech	130-116-398; RRID: AB_2727516
Arginase 1/ARG1/liver Arginase Antibody [Alexa Fluor® 405], polyclonal	Novus	NBP1-32731AF405
Mouse NKG2A/CD159a APC-conjugated Antibody, Clone 705829	R&D Systems	FAB6867A; RRID: AB_10972604
Invitrogen™ CD11b Monoclonal Antibody (M1/70), eFluor™ 506, eBioscience™	ThermoFisher Scientific	69-0112-82; RRID: AB_2637406
Invitrogen™ CD127 Monoclonal Antibody (A7R34), Super Bright™ 645, eBioscience™	ThermoFisher Scientific	64-1271-82; RRID: AB_2744868
Invitrogen™ CD335 (NKp46) Monoclonal Antibody (29A1.4), PerCP-eFluor™ 710, eBioscience™	ThermoFisher Scientific	46-3351-82; RRID: AB_1834441

(*Continued on next page*)

Continued

REAGENT or RESOURCE	SOURCE	IDENTIFIER
Invitrogen™ FOXP3 Monoclonal Antibody (NRRF-30), PE, eBioscience™	ThermoFisher Scientific	12-4771-82; RRID: AB_529580
Invitrogen™ CD11b Monoclonal Antibody (M1/70), eFluor™ 506, eBioscience™	ThermoFisher Scientific	69-0112-82; RRID: AB_2637406
Invitrogen™ iNOS Monoclonal Antibody (CXNFT), Alexa Fluor™ 488, eBioscience™	ThermoFisher Scientific	53-5920-82; RRID: AB_2574423
Chemicals, peptides, and recombinant proteins		
BD Horizon ™ Brilliant Stain Buffer	BD Biosciences	566349
Recombinant murine IL-12 (p70) (carrier free)	BioLegend	577008
Corning™ Regular Fetal Bovine Serum	Fisher Scientific	MT35011CV
Corning™ Cell Culture Buffers: Dulbecco's Phosphate-Buffered Salt Solution 1X	Fisher Scientific	21031CV
Gibco™ Fetal Bovine Serum, certified, heat inactivated, United States	Fisher Scientific	10-082-147
ChromPure Rat IgG, Whole Molecule	Jackson ImmunoResearch	012-000-003
ChromPure Mouse IgG, Whole Molecule	Jackson ImmunoResearch	015-000-003
SeaPlaque™ Agarose	Lonza	50100
Dichloromethane	Millipore Sigma	320269
Resomer® RG 503 H, Poly(D,L-lactide-co-glycolide)	Millipore Sigma	719870
Albumin from mouse serum	Millipore Sigma	A3559
Red Blood Cell Lysis Solution (10x)	Miltenyi Biotech	130-094-183
Sorbitan Monosterate, NF	Spectrum Chemical	SPA63
Polyvinyl Alcohol, USP	Spectrum Chemical	P1180
Polysorbate 80, NF	Spectrum Chemical	PO138
Gibco™ RPMI 1640 Medium	ThermoFisher Scientific	21875034
Invitrogen™ eBioscience™ FoxP3/Transcription Factor Staining Buffer Set	ThermoFisher Scientific	00-5523-00
DL-Limonene	Sigma Aldrich	8.14546
Critical commercial assays		
RNA Agilent Tape Station 4200 High Sensitivity D5000 kit	Agilent	5067-5576, 5067–5577, 5067–5578, 5067–5592, 5067-5593
RNA HS Agilent Tape Station 4200 High Sensitivity D5000 kit	Agilent	5067-5579, 5067–5580, 5067–5592, 5067-5593
Mouse IL-12 (p70) ELISA MAX deluxe ELISA kits	BioLegend	433606
LEGENDplex MU Cytokine Release Syndrome Panel (13-plex) w/VbP	BioLegend	741024
NextSeq 1000/2000 P2 Reagents (100 Cycles) v3	Illumina	20046811
NextSeq 2000 P3 Reagents (100 Cycles)	Illumina	20040559
XT_GX CodeSet FRSMK_DR	NanoString	116003421 (lot – C10552X1)
XT_GXA_P1CS-096	NanoString	116003421 (lot – C10552X1)
nCounter Master Kit	NanoString	100054
NEBNext® Ultra™ II Directional RNA Library Prep Kit for Illumina®	New England Biolabs Inc.	E7760L
NEBNext Poly(A) mRNA Magnetic Isolation Module	New England Biolabs Inc.	E7490L
NEBNext® Globin & rRNA Depletion Kit (Human/Mouse/Rat)	New England Biolabs Inc.	E7750X

(*Continued on next page*)

Continued

REAGENT or RESOURCE	SOURCE	IDENTIFIER
RNeasy Plus Mini Kit	Qiagen Sciences Inc.	74136
Invitrogen™ Qubit™ dsDNA HS and BR Assay Kits	ThermoFisher Scientific	Q32854
Deposited data		
Interferon gamma signaling	Reactome (Garapati[40])	https://reactome.org/content/detail/R-HSA-877300
Interleukin-12 signaling	Reactome (Jupe and Duenas[41])	https://reactome.org/content/detail/R-HSA-9020591
Interleukin-10 signaling	Reactome (Jupe[42])	https://reactome.org/content/detail/R-HSA-6783783
TNF signaling	Reactome (Shamovsky[43])	http://reactome.org/content/detail/R-HSA-75893.7
Chemical and Drug Induced Liver Toxicity	Comparative Toxicogenomics Database (Davis et al.[73])	https://ctdbase.org/detail.go?type = disease&acc = MESH:D056486
Raw and Processed RNA-seq data	This paper	GSE241939
Experimental models: Organisms/strains		
BALB/c mice: 7-8-week-old male and female	The Jackson Laboratory	000651
Oligonucleotides		
NEBNext® Multiplex Oligos for Illumina® (96 Unique Dual Index Primer Pairs)	New England Biolabs Inc.	E6440L
Software and algorithms		
Subread v2.0.1	Liao et al. 2013[128]	https://subread.sourceforge.net
RefSeq	Liao et al. 2014[129]	https://www.ncbi.nlm.nih.gov/refseq/
EdgeR3	Mortazavi et al. 2008[130]	https://bioconductor.org/packages/release/bioc/html/edgeR.html
GSEA_4.3.2	Robinson et al. 2010[131]	http://www.gsea-msigdb.org/gsea/index.jsp
FCS Express [version 7]	*De Novo* Software	https://denovosoftware.com
BioLegend LEGENDplex Data Analysis Software version 2022-07-15	BioLegend	https://legendplex.qognit.com/user/login?next = home
Spectroflo 3.0 software	Cytek Biosciences	https://cytekbio.com/pages/spectro-flo
Cytek Full Spectrum Viewer	Cytek Biosciences	https://spectrum.cytekbio.com
NanoString nCounter Advanced Analysis Software (version 2.0.134)	NanoString	https://NanoString.com/products/analysis-solutions/nsolver-advanced-analysis-software/
NanoString nSolver Analysis Software 4.0	NanoString	https://nanostring.com/products/analysis-solutions/ncounter-analysis-solutions/
Prism9 (version 9.4.1)	GraphPad	https://www.graphpad.com
JMP Pro 16	JMP Statistical Discovery	https://www.jmp.com/en_us/software/predictive-analytics-software.html
Other		
Goldenrod Animal Lancet, 4mm Sterile, 5 trays of 200	Braintree Scientific	GR 4MM
Microvette 100100 UL, round bottom, inner tube Potassium EDTA	Braintree Scientific	MV-100
Pyrex® Vista™ Test Tubes, 15 × 125 mm	Carolina Biological Supply Company	721172
Invitrogen™ OneComp eBeads Compensation Beads	ThermoFisher Scientific	01-1111-42
Invitrogen™ UltraComp eBeads Compensation Beads	ThermoFisher Scientific	01-2222-42
NanoString nCounter custom CodeSet Probes, Abcb11	NanoString	NM_021022.2:1660

(*Continued on next page*)

Continued

REAGENT or RESOURCE	SOURCE	IDENTIFIER
NanoString nCounter custom CodeSet Probes, Abcb4	NanoString	NM_008830.1:1945
NanoString nCounter custom CodeSet Probes, Abcc2	NanoString	NM_013806.2:4600
NanoString nCounter custom CodeSet Probes, Abcc3	NanoString	NM_029600.3:2730
NanoString nCounter custom CodeSet Probes, Alas1	NanoString	NM_020559.2:1034
NanoString nCounter custom CodeSet Probes, Apex1	NanoString	NM_009687.2:289
NanoString nCounter custom CodeSet Probes, ARG1	NanoString	NM_007482.3:626
NanoString nCounter custom CodeSet Probes, Btg2	NanoString	NM_007570.2:50
NanoString nCounter custom CodeSet Probes, Casp3	NanoString	NM_009810.2:630
NanoString nCounter custom CodeSet Probes, CCL2	NanoString	NM_011333.3:415
NanoString nCounter custom CodeSet Probes, CCL3	NanoString	NM_011337.2:219
NanoString nCounter custom CodeSet Probes, CCL4	NanoString	NM_013652.2:200
NanoString nCounter custom CodeSet Probes, Ccng1	NanoString	NM_009831.2:545
NanoString nCounter custom CodeSet Probes, CD19	NanoString	NM_009844.2:1697
NanoString nCounter custom CodeSet Probes, Cd36	NanoString	NM_007643.3:1520
NanoString nCounter custom CodeSet Probes, CD4	NanoString	NM_013488.2:422
NanoString nCounter custom CodeSet Probes, CD8a	NanoString	NM_001081110.2:355
NanoString nCounter custom CodeSet Probes, Cdkn1a	NanoString	NM_007669.4:1670
NanoString nCounter custom CodeSet Probes, CLTA-4	NanoString	NM_009843.3:1475
NanoString nCounter custom CodeSet Probes, CXCL10	NanoString	NM_021274.2:194
NanoString nCounter custom CodeSet Probes, CXCL9	NanoString	NM_008599.4:112
NanoString nCounter custom CodeSet Probes, Cyp1a2	NanoString	NM_009993.3:975
NanoString nCounter custom CodeSet Probes, Cyp1b1	NanoString	NM_009994.1:114
NanoString nCounter custom CodeSet Probes, Eef1g	NanoString	NM_026007.4:338
NanoString nCounter custom CodeSet Probes, Fasn	NanoString	NM_007988.3:6560
NanoString nCounter custom CodeSet Probes, Fmo1	NanoString	NM_010231.3:514
NanoString nCounter custom CodeSet Probes, G6pd	NanoString	NM_008062.2:2030
NanoString nCounter custom CodeSet Probes, Gadd45a	NanoString	NM_007836.1:654
NanoString nCounter custom CodeSet Probes, Gapdh	NanoString	NM_008084.1:755
NanoString nCounter custom CodeSet Probes, GBP2	NanoString	NM_010260.1:1996
NanoString nCounter custom CodeSet Probes, GBP3	NanoString	NM_018734.3:1894
NanoString nCounter custom CodeSet Probes, Gclc	NanoString	NM_010295.2:1102
NanoString nCounter custom CodeSet Probes, Gpx1	NanoString	NM_008160.5:315
NanoString nCounter custom CodeSet Probes, Gsr	NanoString	NM_010344.4:1507
NanoString nCounter custom CodeSet Probes, HAVCR2	NanoString	NM_134250.2:134
NanoString nCounter custom CodeSet Probes, Hmox1	NanoString	NM_010442.2:610
NanoString nCounter custom CodeSet Probes, Hprt	NanoString	NM_013556.2:30
NanoString nCounter custom CodeSet Probes, Icam1	NanoString	NM_010493.2:2195
NanoString nCounter custom CodeSet Probes, IFNG	NanoString	NM_008337.3:402
NanoString nCounter custom CodeSet Probes, IL10	NanoString	NM_010548.2:250
NanoString nCounter custom CodeSet Probes, IL12RB1	NanoString	NM_008353.2:2765
NanoString nCounter custom CodeSet Probes, IL1B	NanoString	NM_008361.3:108
NanoString nCounter custom CodeSet Probes, Il2rg	NanoString	NM_013563.3:566
NanoString nCounter custom CodeSet Probes, IL6	NanoString	NM_031168.1:200
NanoString nCounter custom CodeSet Probes, IRF1	NanoString	NM_008390.2:845
NanoString nCounter custom CodeSet Probes, ITGAM	NanoString	NM_008401.2:155

(*Continued on next page*)

Continued

REAGENT or RESOURCE	SOURCE	IDENTIFIER
NanoString nCounter custom CodeSet Probes, ITGAX	NanoString	NM_021334.2:327
NanoString nCounter custom CodeSet Probes, LAG3	NanoString	NM_008479.1:1700
NanoString nCounter custom CodeSet Probes, Lpl	NanoString	NM_008509.2:802
NanoString nCounter custom CodeSet Probes, Ly6g	NanoString	XM_909927.2:91
NanoString nCounter custom CodeSet Probes, Mt2	NanoString	NM_008630.2:105
NanoString nCounter custom CodeSet Probes, NCR1	NanoString	NM_010746.3:995
NanoString nCounter custom CodeSet Probes, NOS2	NanoString	NM_010927.3:1541
NanoString nCounter custom CodeSet Probes, Nqo1	NanoString	NM_008706.5:430
NanoString nCounter custom CodeSet Probes, PD-L1	NanoString	NM_021893.2:515
NanoString nCounter custom CodeSet Probes, Polr1b	NanoString	NM_009086.2:2795
NanoString nCounter custom CodeSet Probes, Polr2a	NanoString	NM_001291068.1:2768
NanoString nCounter custom CodeSet Probes, Ppara	NanoString	NM_011144.2:1345
NanoString nCounter custom CodeSet Probes, Rb1	NanoString	NM_009029.2:1590
NanoString nCounter custom CodeSet Probes, Rbp1	NanoString	NM_011254.5:709
NanoString nCounter custom CodeSet Probes, Rpl19	NanoString	NM_009078.1:20
NanoString nCounter custom CodeSet Probes, Sdha	NanoString	NM_023281.1:250
NanoString nCounter custom CodeSet Probes, Serpine1	NanoString	NM_008871.2:1822
NanoString nCounter custom CodeSet Probes, SOCS1	NanoString	NM_009896.2:440
NanoString nCounter custom CodeSet Probes, SOCS3	NanoString	NM_007707.3:1952
NanoString nCounter custom CodeSet Probes, Srebf1	NanoString	NM_011480.1:1145
NanoString nCounter custom CodeSet Probes, STAT1	NanoString	NM_001205313.1:430
NanoString nCounter custom CodeSet Probes, STAT3	NanoString	NM_213659.2:1360
NanoString nCounter custom CodeSet Probes, STAT4	NanoString	NM_011487.4:1816
NanoString nCounter custom CodeSet Probes, Thrsp	NanoString	NM_009381.2:760
NanoString nCounter custom CodeSet Probes, TNF	NanoString	NM_013693.2:514
NanoString nCounter custom CodeSet Probes, Txnrd1	NanoString	NM_015762.2:2245

RESOURCE AVAILABILITY

Lead contact

Further information and requests for datasets generated and/or analyzed in the current study should be directed to the lead contact, Dr. Brock. A Lindsey, MD (blinds10@jh.edu).

Materials availability

This study did not generate new and/or unique reagents.

Data and code availability

(1) RNA-seq data have been deposited at GEO and are publicly available as of the date of publication. Accession numbers are listed in the key resources table. This paper also utilizes existing, publicly available data. These accession numbers and/or URLs for these datasets are listed in the key resources table.
(2) There is no associated original code used for data analysis in this manuscript.
(3) All other datatypes and additional information required to reanalyze the data reported are available from the lead contact upon reasonable request.

EXPERIMENTAL MODEL AND STUDY PARTICIPANT DETAILS

All animal procedures performed were approved by the WVU Institutional Animal Care and Use Committee. Healthy, 7-8-week-old male and female BALB/c (#000651) were obtained from The Jackson Laboratory (Bar Harbor, ME). Mice were housed individually in ventilated Allentown cages, within specific pathogen-free facilities, on corncob bedding with 12-h light/dark cycles. Mice had *ad libitum* access to irradiated Teklad

Global 18% Protein Rodent Diet (2918-060122M) with guaranteed analysis of crude protein no less than 18.0%, crude fat no less than 5.0%, and crude fiber no more than 5.0% (Madison, WI). Mice were assigned to the respective treatment groups by simple randomization upon arrival and given an approximate 2-week acclimation period before receiving first treatments.

METHOD DETAILS

Experimental design

To perform an immunotoxicology assessment of recombinant murine interlekin-12-loaded PLGA nanospheres (IL12ns), we compared the resulting systemic immune responses from various IL-12 treatment regimens in healthy, 7–8-week male/female BALB/c mice via 7 serial blood sampling timepoints (Figure 1). Timepoints include baseline (T1), 12-h (T2), day 4 (T3), day 8 (T4), day 11 (T5), day 15 (T6), and day 18 (T7), at which time mice were humanely euthanized following cardiac puncture for full necropsy. Five (5) treatment groups, each with 8 male and 8 female mice, examined four different IL-12 dosing strategies, (1) 10,000 ng/kg/day daily [maximum tolerable dose (MTD)], (2) 10 mg IL12ns delivering ~1600 ng/kg/day rmIL-12, (3) 0.1 mg IL12ns delivering ~16 ng/kg/day rmIL-12, and (4) 0.001 mg IL12ns delivering ~0.16 ng/kg/day rmIL-12, alongside (5) a non-treatment, saline control (Figure 1A). Daily administration of 16,000 ng/kg/day is considered the toxic dose for mice, as extreme weight loss ultimately required humane euthanasia 8–10 days thereafter.[126] Therefore, 10,000 ng/kg/day was chosen as the maximum tolerable dose (MTD) so that effects of a bolus IL-12 could be examined while ensuring survival of animals to the humane endpoint of 18 days (T7). At each sampling timepoint, peripheral blood was collected via cheek bleed (~80 μL) for analysis via an immune diagnostic platform (IDP) consisting of peripheral blood mononuclear cell (PBMC) spectral flow cytometric analysis, plasma cytokine/chemokine analysis via BioLegend (San Diego, CA) LEGENDplex, and bulk PBMC RNA sequencing (Figure 1B). At day 18 (T7, euthanasia), peripheral blood was collected via cardiac puncture alongside necropsy to harvest heart, liver, spleen, lungs, and kidneys for histopathological analysis by two, independent board-certified pathologists and a veterinarian medical doctor. RNA was then isolated from FFPE liver, spleen, and lung specimens for NanoString nCounter gene expression analysis using a custom pro-inflammatory panel (Figure 1A).

IL12ns and rmIL-12 administration

IL12ns, free rmIL-12 (MTD), or saline was administered via intraperitoneal (i.p.) injection using either a 1 inch, 18-gauge (IL12ns and saline) or 1/2 inch, 27-gauge needle (free rmIL12) with luer-lock 1 mL syringe. IL12ns and saline were injected weekly, 12 h before timepoints T2, T4, and T6, while the MTD was administered daily (Figure 1A). Briefly, mice were manually restrained with the body tilted downward. Injections were administered into the peritoneal cavity using an injection site in the lower quadrant of the abdomen, lateral to the midline. Importantly, all doses were delivered precisely 12 h prior to the blood draw the following morning. This timing allowed for analysis of the initial stimulatory immune response (particularly the effectors IFN-γ, CXCL9, and CXCL10 downstream of the IL-12 signaling pathway) following IL-12 injection.[31] The 6-to-24-h period post-injection was deemed critical in human clinical trials which revealed that repeated administration of IL-12 resulted in decreased IFN-γ release with subsequent injections.[23] The weight adjusted MTD dose was injected immediately following a daily weight measurement.

Peripheral blood collection

Without anesthesia, mice were cheek bled with a 4 MM Braintree Scientific (Braintree, MA) Goldenrod Animal Lancet for collection of 3–4 drops of blood (~80 μL, however, weight adjusted) into a 100 μL microvette EDTA tube at all timepoints (Figure 1A). Once collected, decreasing pressure on the vein (by releasing the scruff hold) stopped the bleeding. If the bleeding continued, pressure was gently applied with a gauze pad until blood clotted. To perform blood draws quickly and effectively within a 30-min time frame, the study was split into a total of four 20-animal groups with equal representation of control and experimental arms.

Synthesis of IL12ns

IL12ns were prepared via the double-emulsion solvent evaporation (DESE) method with ultrasonication as previously described.[30,132] First, under sterile conditions, the primary emulsion was formed using an Omni International (Kennesaw, GA) Sonic Ruptor 250 microprobe sonicator set at 50% power to agitate 150 μL of aqueous (aq) solution (including 12.5 μg rmIL-12), 250 mg Resomer RG 503 H, Poly(D,L-lactide-co-glycolide), and 14% w/w Sorbitan Monostearate dissolved in 1.5 mL dichloromethane (DCM) for 10 s in a Pyrex Vista test tube held on ice bath. The 150 μL aq solution contained 136 μL of 10% w/v mouse serum albumin (MSA) and 14 μL of rmIL-12 (BioLegend). The primary emulsion was transferred to a second Pyrex Vista test tube containing 1% w/v polyvinyl alcohol (PVA) and 4% w/v Polysorbate 80 in deionized water, and the solution was sonicated on ice at 50% for an additional 10 s to create the double emulsion. The double emulsion was subsequently stirred for a minimum of 3 h at 1000 rpm to allow organic solvent evaporation, washed via resuspension and ultracentrifugation at 47,807 g three times for 40 min, flash-frozen in liquid nitrogen, lyophilized using the Labconco (Fort Scott, KS) 700802000 FreeZone 8L −50°C Benchtop Freeze Dryer, and stored in a vacuum desiccator. Importantly, IL12ns batches were prepared weekly to ensure quality controlled batches were injected at dosing timepoints.

IL12ns characterization

The morphology of modified IL12ns was determined by scanning electron microscopy (SEM) (Nanocomposix, San Diego, CA) Hitachi (Tokyo, Japan) S-4700 FE-SEM as previously described.[30] To determine IL12ns elution profile, a 0.6% Lonza (Allendale, NJ) SeaPlaque Agarose gel

was prepared according to manufacturer specifications and previous publication.[133] Briefly, IL12ns were prepared by resuspending 1 mL of lyophilized particle in D-PBS before aliquoting 10 mg of IL12ns into a 1.5 mL tube. IL12ns were spun for 15 min at 10,000 x g at 4°C before pouring off supernatant, leaving pelleted particles. Upon cooling the gel to 37°C, 10 mg of IL12ns were resuspended in 1 mL of SeaPlaque agarose gel and plated into a 24-well standard cell culture plate. Agarose/particle was then gelled at 4°C for minimum of 15 min before incubating in standard cell culture conditions (37°C, 5% CO_2) for an additional 15 min. One mL of release buffer [10% fetal bovine serum (FBS) in D-PBS with 1% penicillin/streptomycin] was added on top of the gel to begin the elution study. Samples were collected every 24 h by gently removing the supernatant above the gel (now containing eluted rmIL-12) and replacing 1 mL of release buffer. This collected supernatant was then analyzed by enzyme-linked immunosorbent assay (ELISA) for rmIL-12 concentration using murine IL-12 ELISA Max Deluxe kit (BioLegend). Concentration (mg/mL) from each IL12ns batch was calculated by weighing dried IL12ns product after lyophilizing 1 mL of suspended IL12ns in a pre-weighed 1.5 mL tube for 12 h. IL12ns yield (mg/mL) was calculated by multiplying this concentration (mg/mL) by the total volume of which the IL12ns batch was resuspended (4 mL). Encapsulation efficiency (EE) of IL12ns was determined as previously indicated.[30] Dynamic light scattering (DLS) analysis was performed on a Malvern Panalytical (Worcestershire, UK) Zetasizer Nano ZS instrument (Figure S1). All values are presented as an average ±standard error of the mean (SE) (n = 4 or 6). Importantly, to pass quality assessment, a newly synthesized IL12ns batch was eluted for 48 h before quantifying IL-12 release. Both the 24- and 48-h measurements must have fallen within a standard error of the mean (SE) of 10% (in comparison to a set standard) to pass quality control and be injected thereafter.

Clinical moribundity and mortality observations

Mice were monitored daily over the course of 18 days using a standard stress assessment for signs of morbid (ill) and moribund (near death) status, which considers overall appearance, behavior, weight change, as well as feeding patterns. Mice that met majority criteria as morbid [hunched posture (<48 h), ruffled hair coat, erection of hair or fur, lack of grooming behavior, sunken eyes, with or without discharge, acute diarrhea or constipation (<48 h), respiration rate increased or decreased, respiration effort mildly increased, rapid weight loss of ≥10% body weight, decreased food intake, mild dehydration or decreased water intake, unsteady gait or lameness (not experimentally induced/expected), ulcerative dermatitis, and moderate to severe fight wounds] were identified and monitored closely for acceleration into moribund status [hunched posture (≥48 h), muscle atrophy and signs of severe lethargy or unresponsiveness, inability to remain upright, prolonged diarrhea or constipation (≥48h), severe respiratory distress (agonal breathing) which is unresponsive to treatment, cyanosis (blue color to skin or mucus membranes), rapid and spontaneous weight loss ≥20% body wt./emaciation, frank bleeding, unresponsive to treatment, clinical dehydration (>10%) and/or prolonged lack of food intake (≥48h), one or more skin ulcers that do not heal, self-mutilation that is sustained or debilitating, hematological or biochemical values indicative of organ failure] for which the animal then met criteria for early euthanasia. If a mouse had two failed moribundity observations (now mortality observations), they were humanely euthanized before scheduled endpoint euthanasia. To prevent injury at the injection site, the side of peritoneal cavity for which the injection was administered was swapped (left or right) with each subsequent injection. Each injection site was evaluated pre- and post-injection to ensure there were no signs of infection, scarring, bruising, or irritation. Rapid weight loss (>10% from previous measurement) was a morbid observation that was closely monitored by daily weight measurements. Previously published data suggested significant weight loss as the driving factor for early euthanasia with IL-12 injection at toxic doses.[126]

Spectral flow cytometric analysis

Peripheral blood mononuclear cells (PBMCs) were analyzed via a 16-marker myeloid and 23-marker lymphoid panel on the Cytek Biosciences (Fremont, CA) Aurora at each peripheral blood sampling timepoint using the antibodies outlined in the key resources table and the appended gating strategy (Figure S7). The lymphoid and myeloid panels were designed using Cytek Full Spectrum Viewer to achieve a complexity score of 5.63 and 4.55, respectively, before full panel titration using calculated staining indexes. Briefly, blood was prepared into a PBMC single cell suspension using Miltenyi Biotec (Gaithersburg, MD) Red Blood Cell Lysis 10x solution with a modified laboratory protocol. For each staining day, a staining plate contained individual PBMCs for full staining with all dyes and antibodies, as well as PBMCs from euthanized instrument control animals (n = 2) to generate no stain controls, single-stain samples for each fluorophore in the staining panel (sometimes performed on compensation beads), and fluorescence minus one (FMO) controls for specific fluorophores. A live/dead master mix sufficient for the number of samples plus one was prepared and added to each sample, live/dead single stain control, and all necessary FMO controls before incubation in the dark for 30 min at 4°C. Following a wash by adding 100 μL of PBS to each well before centrifugation at 1200 rpm at 4°C for 5 min, a Fc blocking master mix with volume sufficient for the number of samples plus one using 0.4 μL of Jackson Immunoresearch (West Grove, PA) ChromPure Rat IgG, 0.4 μL of ChromPure Mouse IgG, and 19.2 μL D-PBS was added to each sample well before incubation in the dark for 30 min at 4°C. Samples were again washed before cell surface staining with a freshly prepared surface stain master mix sufficient for the number of full-stain samples plus one containing 50 μL Brilliant Staining Buffer and each surface-staining antibody. To FMO control wells, each antibody-fluorophore conjugate in the staining panel minus one was added to instrument control PBMCs. Samples were then incubated in the dark for 30 min at 4°C before two washing steps as previously described. Then, 200 μL of prepared fixation reagent was added to all sample wells and incubated in the dark for 30 min at 25°C. Samples were then washed by adding 200 μL of 1x permeabilization buffer to each well and centrifuging at 1200 rpm, 25°C, for 5 min. Following decantation, an intracellular stain master mix sufficient for the number of samples plus one containing 30 μL permeabilization buffer and each intracellular-staining antibody was added to each full-stain sample well, appropriate single-stain, and FMO control wells. Samples were again incubated in the dark for 30 min at 4°C before washing two times by adding 200 μL of 1x permeabilization buffer to each well and centrifuging at 1200 rpm, 25°C, for exactly 5 min. Finally, cells were resuspended in

200 μL D-PBS and transferred to a clean 96-well plate that was then sealed and packed for overnight shipping to UVA Flow Cytometry Core (RRID: SCR_017829, Charlottesville, VA) for spectral flow cytometric analysis on the Cytek Aurora (Cytek Biosciences) equipped with 355nm, 405nm, 488nm, 561nm, and 633nm lasers. Acquisition was performed using the automated sample loader set to acquire 200 μL of each sample stained and prepared in 96-well plates. For analysis, data were unmixed using Spectroflo 3.0 software (Cytek Biosciences) (Figure 1B). Unmixed flow cytometry standard (FCS) files were analyzed using FCS Express [version 7, *De Novo* Software (Pasadena, CA)] and pre-determined gating strategies. Plots and statistics (% of all live cells) were exported using the Batch Export function from FCS Express to Microsoft Excel (Redmond, VA) before further statistical analysis via JMP (JMP Statistical Discovery, Cary, NC) [version Pro16] and graphical representation using GraphPad (San Diego, CA) Prism [version 9.4.1].

Plasma analysis via BioLegend LegendPlex

Peripheral plasma cytokine and chemokine analyses at all blood collection timepoints were conducted using the BioLegend LEGENDplex Cytokine Release Syndrome Panel for quantification of IFN-γ, IL-10, CCL4 (MIP-1β), IFN-a, CXCL9 (MIG), CXCL10 (IP-10), TNF-α, IL-6, VEGF, IL-4, CCL3 (MIP-1α), CCL2 (MCP-1), and GM-CSF concentration according to manufacturer specifications for a v-bottom 96-well plate. Briefly, following collection of peripheral blood in 100 μL Microvette EDTA tubes, plasma was isolated from ~50 μL of peripheral blood by centrifuging for 20 min at 1,000 × g within 30 min of blood collection. Plasma was then stored at −80°C for later analysis. Each plasma sample underwent one freeze/thaw cycle and was processed at a 1:2 dilution according to manufacturer specifications. Multiplexed-plasma samples were then read on the Life Technologies Attune Nxt (ThermoFisher Scientific) at the UVA Flow Cytometry Core Facility (RRID: SCR_017829). Samples were gated, processed, and analyzed using the online BioLegend LEGENDplex Data Analysis Software [version 2022-07-15] before statistical analysis via JMP [version Pro 16] and graphical representation using GraphPad Prism9 [version 9.4.1] (Figure 1B).

RNA extraction, library preparation, and next-generation sequencing of PBMCs

Total RNA was isolated from PBMCs collected at all sampling timepoints following preparation into single cell suspension using the Qiagen (Germantown, MD) RNeasy Plus Mini Kit. Total RNA sample quality was assessed for purity by the Thermo/Spectronic BioMate3 (Spectrophotomer, ThermoScientific) using standard OD 260/280 range before being stored in 30 μL RNase free water at −80°C. Samples were then processed by the UVA Genome Analysis and Technology Core, RRID:SCR_018883 using Standard Operating Procedures for an n = 3 for each group (10 mg IL12ns, 0.1 mg IL12ns, MTD, and saline control) for both males and females at all sampling timepoints for a total of 168 total RNA samples. Total RNA quality was checked using the Agilent (Santa Clara, CA) Tape Station 4200 along with either the RNA (5067–5576, 5067–5577, 5067–5578) or RNA HS (5067–5579, 5067–5580) kit as appropriate to the RNA concentration provided and as described by the manufacturer's protocols. RNA-seq libraries were prepared using New England Biolab's (Ipswich, MA) NEBNext Poly(A) mRNA Magnetic Isolation Module (E7490L), Globin & rRNA Depletion Kit (E7750X), Ultra II Directional RNA Library Prep Kit for Illumina (E7760L), and Multiplex Oligos for Illumina (E6440L) according to the manufacturer's instructions. Libraries were checked for quality, size, and concentration using the Agilent Tape Station 4200 High Sensitivity D5000 kit (5067–5592, 5067–5593) and Qubit 3.0 ThermoFisher dsDNA HS Assay Kit (Q32854). Libraries were pooled at equimolar concentrations and sequenced using Illumina's NextSeq 2000 on one P2-100 (20046811) kit and four P3-100 (20040559) kits according to the manufacturer's instructions (Figure 1B).

Bulk PBMC RNA-seq analysis

Following concatenation of FASTQ files each sequencing run (n = 2), alignment of paired-end short reads to the reference mouse genome (mm10) was performed with subread v2.0.1.[128] Reads aligned to RefSeq transcripts were summarized at the gene level by feature counts.[129] The gene expression level was measured by reads per kilobase of exon model per million mapped (RPKM).[130] Differentially expressed (DE) genes were predicted by EdgeR3[131] with FDR <0.05, fold change >1.5, and CPM (count per million; log2) > 0. The resulting logFc's were then used for targeted Gene Set Enrichment Analysis (GSEA) [version GSEA_4.3.2] for analysis of four Reactome[39] gene sets, including Interleukin-12 signaling,[41] Interferon gamma signaling,[40] Interleukin-10 signaling,[42] and TNF signaling.[43] Unbiased GSEA of both the Reactome[39] and Hallmark[44] gene sets were also performed. RPKMs for those related/matching genes from flow cytometric and cytokine/chemokine panels, as well as the above Reactome pathways, were then analyzed using JMP Pro 16, with statistical significance set at $p < 0.01$.

Necropsy and histopathology assessment

At day 18 euthanasia (T7) (Figure 1A), following cardiac puncture exsanguination, mice were humanely euthanized via cervical dislocation under anesthesia. Necropsy for collection of heart, liver, spleen, lungs, and kidneys was then performed. Each tissue was immediately placed in 5 mL of FormaFix (prepared per manufacturer protocol) before serially transecting, paraffin embedding, slicing with a microtome at 10 μm, and placement on glass slides. Tissues were analyzed by two independent board-certified pathologists at both the WVU School of Medicine (WVUSOM) and University of Pittsburgh Medical Center (UPMC), Departments of Pathology, as well as a Veterinarian Medical Doctor at the University of Pittsburgh School of Medicine, blinded to both group and outcome.

For evaluation of the liver, specimens were examined for the following: portal inflammation (predominant cell type, granulomas present), lobular inflammation (predominant location, predominant cell type, granulomas present), bile duct inflammation (cholangitis), steatosis (predominantly microvesicular steatosis), cholestasis, hepatocyte single cell necrosis, hepatocyte grouped (confluent) necrosis, hepatocyte ballooning (hydropic change), hepatocyte mitotic activity, and other hepatocyte changes (e.g., dysplasia, pigment deposition, nuclear or

cytoplasmic inclusions). If present, bile duct injury (nuclear displacement, eosinophilia, vacuolization), ductopenia, bile ductular reaction/proliferation, sinusoidal congestion, sinusoidal dilatation, vascular thrombosis, vascular inflammation, fibrosis, or tumor was specified.

For the spleen, specimens were examined for hypoplasia, increased apoptosis, white pulp atrophy, red pulp telangiectasis, red pulp atrophy, red pulp congestion, increased erythrophagocytosis, fibrosis, increased pigment, increased macrophage aggregates, increased plasma cells, white pulp hyperplasia, red pulp adipocyte hypercellularity, increased mast cells, peri-splenic inflammation, stromal cell hyperplasia, and increased extramedullary hematopoiesis (EMH).

For the kidneys, specimens were examined for the following: cortical interstitial inflammation (predominant cell type, granulomas present), medullary interstitial inflammation (predominant cell type, granulomas present), tubular inflammation (tubulitis) (predominant cell type, involved tubule location), glomerulitis (predominant cell type), arterial inflammation (arteritis), tubular degeneration/necrosis (indicating the areas involved with tubular injury), tubular vacuolization, vacuolization pattern, tubular casts, cast type, tubular dilatation, interstitial renal hemorrhage, renal infarct, vascular thrombosis, vascular necrosis, vascular smooth muscle vacuolization, glomerulopathy, or glomerulonephritis.

For the lung, specimens were examined for interstitial inflammation (predominant inflammatory cell type, granulomas present), airway (bronchial/bronchiolar) inflammation, alveolar injury (if inflammation is present, predominant cell type, indicate granuloma presence), vascular thrombosis, vascular inflammation (vasculitis), vascular necrosis, pulmonary fibrosis, and presence of tumor.

Finally, for evaluation of the heart, specimens were analyzed for endomyocardial inflammation (predominant cell type, granuloma present), myocardial necrosis, myocardial fibrosis, and coronary artery changes (including thrombosis, arteritis, atherosclerosis).

For quantification of histopathological findings, total pathology (total path), total necrosis, and total inflammation scores were calculated. Presence of the histopathological finding was indicated as a "1", with absence of the finding indicated as a "0". The total necrosis score was calculated by summing both necrotic and fibrotic histopathological findings for each specimen. The total inflammation score was calculated by summing those non-necrotic and non-fibrotic histopathological findings. The total pathology score equals the summation of both total necrosis and inflammation scores. Data were then transformed to generate non-zero findings in Microsoft Excel using the below formula where *N* represents number of animals within each group observed:

$$Transformed\ Histopathological\ Finding = \frac{(\#\ of\ histopathological\ findings)+1}{N+2}$$

Following this data transformation, histopathological findings were then normalized to background by dividing the total pathology (total path), total necrosis, and total inflammation scores for each experimental animal by the average total pathology (total path), total necrosis, or total inflammation score for the respective matched-sex saline control. This normalization was completed for each of the three independent pathological assessments and accounts for any subjectivity in analysis by the three independent reviewers.[134] Normalized scores for male and female experimental groups were then plotted within violin plots using GraphPad Prism9 [version 9.4.1]. Additional pathological findings can be found in File S4 – Additional Pathological Findings.pdf.

RNA extraction from formalin-fixed, paraffin embedded liver, spleen, and lung specimens

A total of 72 blocks of FFPE mouse tissue (24 liver, lung, and spleen specimens) representing an n = 3 for each group (10 mg IL12ns, 0.1 mg IL12ns, MTD, and saline control), both male and female, were used for RNA extraction. Four slices of 10 μm thickness from each selected block were deparaffinized using DL-Limonene (MilliporeSigma, Burlington, MA) and digested with proteinase K (Qiagen). RNA was then isolated using Qiagen RNeasy Plus Mini Kit according to manufacturer protocol. The final volume of extracted RNA was 14 μL. RNA concentration and purity were assessed using a NanoDrop instrument. Sample concentration was measured at 260 nm and 280 nm. The ratio of optical density 260/280 and 260/230 were used to test for protein and phenol contamination, respectively.

NanoString nCounter analysis of formalin-fixed, paraffin-embedded liver, spleen, and lung specimens

A custom 42-marker nCounter CodeSet panel including NanoString (Seattle, WA) probes for *Alas1, Arg1, Ccl2, Ccl3, Ccl4, CD19, PD-L1, CD4, CD8a, CTLA-4, Cxcl10, Cxcl9, Eef1g, G6pd, Gapdh, Gbp2, Gbp3, Havcr2, Hprt, Ifng, Il10, Il12rb1, Il1b, Il2rg, Il6, Irf1, Itgam, Itgax, Lag3, Ly6g, Ncr1, Nos2, Polr1b, Polr2a, Rpl19, Sdha, Socs11, Socs3, Stat1, Stat3, Stat4, and Tnf* was designed for targeted gene expression analysis of FFPE-isolated RNA from liver, spleen, and lung specimens collected at euthanasia. An additional custom 30-marker nCounter CodeSet Plus panel including probes for *Abcb11*, Abcb4, *Abcc2, Abcc3, Apex1, Btg2, Casp3, Ccng1, Cd36, Cdkn1a, Cyp1a2, Cyp1b1, Fasn, Fmo1, Gadd45a, Gclc, Gpx1, Gsr, Hmox1, Icam1, Lpl, Mt2, Nqo1, Ppara, Rb1, Rbp1, Serpine1, Srebf1, Thrsp, Txnrd1* was also designed for targeted gene expression analysis of the same FFPE-isolated RNA from liver specimens for analysis of drug-induced liver toxicity. Importantly, *Alas1, Eef1g, G6pd, Gapdh, Hprt, Il2rg, Polr1b, Polr2a, Rip19, and Sdha* were included as reference or housekeeping genes for each tissue analyzed. NanoString probes are made with target-specific sequences and tag-specific sequences at 5′ and 3′ tailing ends. The RNA samples (150 ng) were incubated for 24 h at 65°C in a hybridization buffer containing the CodeSet (reporter and capture probes). Hybridized samples were processed using the Prep Station high sensitivity protocol, 3 h per 12-sample cartridge. The Prep Station purifies the RNA/probe complexes and places them in a cartridge where they are immobilized and aligned for data collection. Data acquisition was carried out using the NanoString nCounter Digital Analyzer with the 'Max' Field of View (FOV) setting to acquire 555 images per sample in a 5-h scan per cartridge as previously described.[135,136]

QUANTIFICATION AND STATISTICAL ANALYSIS

Statistical power analysis determined that a minimum of eight mice (per sex) was sufficient to detect immunophenotypic differences in NK cells via spectral flow cytometry between treated and untreated mice, to obtain 80% power, a desired p value of 0.05, and an anticipated standard deviation (STDEV) of 33%. First, for spectral flow cytometric, cytokine, and chemokine analyses, data were analyzed using a two-factor analysis of variance (ANOVA) with interaction stratified by each sex and marker. Our interest focused on the timepoint by group interaction. A Bonferroni correction was applied separately within each flow cytometric, cytokine, or chemokine analysis to account for the large number of significance tests completed. Bonferroni correction factor was calculated using a multiple of the number of cellular population/markers (myeloid – 112, lymphoid – 134, NK cells – 159 markers, cytokine/chemokine – 13), timepoints (7), and sex (2) for each analysis. Only those cellular populations/markers deemed statistically significant in the above analysis were subsequently analyzed using a one-factor ANOVA with group as the factor of interest. Those analyses were performed separately for each timepoint, sex, and cellular population/marker. Post hoc pairwise means comparisons were done using Tukey's HSD procedure. A further Bonferroni correction was used to adjust for the large number of inferences tested, with statistical significance for all remaining cellular populations/markers set at $p < 0.0001$ (JMP Pro 16, Files S1 and S3. Error bars represent standard error of the mean (SE). RNA-Seq data generated from the study were deposited to GEO with an accession # of GSE241939. For bulk PBMC RNA-seq analysis, those GSEAs with an NES >1.6 and FDR <0.05 were considered statistically significant (version GSEA _4.3.2). Additionally, a one-factor ANOVA with post hoc pairwise means comparison by Tukey's HSD procedure was used to compare gene expression (RPKM) between experimental groups, with significance set at $p < 0.01$ (JMP Pro 16, File S2. For histopathological analysis, the total pathology (total path), total necrosis, and total inflammation scores were compared between experimental groups using a one-way ANOVA with statistical significance set at $p < 0.05$ [GraphPad Prism9 (version 9.4.1)]. NanoString nCounter analysis was performed using NanoString nSolver Analysis Software 4.0. Following selection and annotation, samples were processed using background thresholding, with a threshold count value of 20, positive control normalization, and CodeSet content normalization using housekeeping genes to compute a normalization factor. Low count data were omitted at this threshold count value of 20 with an observation frequency of 0.99. Housekeeping selection for each specimen was made using Geonorm standards within the nCounter Advanced Analysis software (version 2.0.134). Differentially expressed genes between treatment groups and saline controls were calculated using the nCounter Advanced Analysis software. To estimate differential expression, either the mixed negative binomial model using the mle function to run the Wald test, the simplified negative binomial model using the glm.nb function, or the log-linear model using the lm function were deployed to determine estimated log fold-change. This estimated log fold-change and Benjamini-Yekutieli adjusted p value (* = $p < 0.05$, ** = $p < 0.01$, *** = $p < 0.001$, **** = $p < 0.0001$) were then calculated for each experimental group in comparison to saline controls. Log2 normalized expressions for each experimental group are graphed using GraphPad Prism9 (version 9.4.1). NanoString nCounter quality control for each 12-sample analysis can be seen in File S5. Due to the known differences in immune response between males and females,[127,137] each analysis was completed on both sexes independently. Statistical parameters are reported in the accompanying figure legend.